

**DETERMINATION OF TREE HEIGHTS  
USING UNMANNED AIR VEHICLES**

**Anıl Can BİRDAL**

**MASTER OF SCIENCE THESIS**

**Remote Sensing and Geographic Information Systems Program**

**Supervisor: Assist. Prof. Dr. Uğur AVDAN  
Second Supervisor: Assoc. Prof. Dr. Tarık TÜRK**

**Eskişehir**

**Anadolu University**

**Graduate School of Science**

**July, 2016**

*This thesis is financially supported by Anadolu University Scientific Research Projects (Project No: 1407F356).*

*Bu tez çalışması Anadolu Üniversitesi Bilimsel Araştırma Projeleri (Proje No: 1407F356) tarafından desteklenmiştir.*

## FINAL APPROVAL OF THESIS

This thesis titled “Determination of Tree Heights Using Unmanned Air Vehicles” has been prepared and submitted by Anıl Can Birdal in partial fulfillment of the requirements in “Anadolu University Directive on Graduate Education and Examination” for the Degree of Master of Science in Remote Sensing and Geographical Information Systems Program has been examined and approved on 22/07/2016.

<b>Committee Members:</b>		<b>Singature</b>
<b>Member (Tez Danışmanı)</b>	: Assist. Prof. Dr. Uğur AVDAN	.....
<b>Member (Eşdanışman)</b>	: Assoc. Prof. Dr. Tarık TÜRK	.....
<b>Member</b>	: Assoc. Prof. Dr. Murat UYSAL	.....
<b>Member</b>	: Assist. Prof. Dr. Emrah PEKKAN	.....
<b>Member</b>	: Assist. Prof. Dr. Muammer TÜN	.....

.....

**Date**

.....

**Director**

**Graduate School of Sciences**

## ABSTRACT

### DETERMINATION OF TREE HEIGHTS USING UNMANNED AIR VEHICLES

Anıl Can BİRDAL

Department of Remote Sensing and Geographic Information Systems  
Graduate School of Sciences, July, 2016

Supervisor: Assist. Prof. Dr. Uğur AVDAN

(Co-Supervisor: Assoc. Prof. Dr. Tarık TÜRK)

Unmanned aerial vehicles (UAV) have been widely used in a variety of fields in the last decade. In forestry, with different sensors, they have been used to estimate tree heights and crowns. This approach with a consumer-grade camera onboard system is becoming popular because it is cheaper and faster than traditional photogrammetric methods and UAV-Light Detecting and Ranging (UAV-LiDAR) systems. In this study, UAV-based imagery reconstruction, processing, and local maximum filter methods are used to obtain individual tree heights from an urban forest area which consists mostly of coniferous trees as scots and black pines and considered as very opened canopy. A low-cost onboard camera and a UAV with a 96-cm wingspan made it possible to acquire high resolution aerial images (6.41 cm average ground sampling distance), ortho-images, Digital Elevation Models (DEM), and point clouds in one flight. Canopy Height Models (CHM), obtained by extracting the Digital Surface Model (DSM) from the Digital Terrain Model (DTM), were filtered locally based on the pixel-based window size using the provided algorithm. For accuracy assessment, ground-based tree height measurements were made. There was a high 94 per cent correlation and a root mean square error of 28 cm. This study highlights the accuracy of the method and compares favorably to more expensive methods.

**Keywords:** Unmanned Aerial Vehicles; Tree Height Detection; Photogrammetry; Image Processing; Local Maximum Filter; Consumer-grade Cameras

## ÖZET

### AĞAÇ YÜKSEKLİKLERİNİN BELİRLENMESİNDE İNSANSIZ HAVA ARAÇLARININ KULLANIMI (ESKİŞEHİR KENT ORMANI ÖRNEĞİ)

Anıl Can BİRDAL

Uzaktan Algılama ve Coğrafi Bilgi Sistemleri Anabilim Dalı  
Anadolu Üniversitesi, Fen Bilimleri Enstitüsü, Temmuz, 2016

Danışman: Yrd. Doç. Dr. Uğur AVDAN

İkinci Danışman: Doç. Dr. Tarık TÜRK

Geçtiğimiz on yıl içinde insansız hava araçları, çeşitli çalışma alanlarında sıkça kullanılmaya başlamıştır. Ormancılık sektöründe, çeşitli alıcılar ile ağaç yüksekliklerinin hesaplanması ve taçlarının kestirimi için kullanılmaktadırlar. Bu tezde kullanılan yöntem olan tüketici sınıfı bir kameranın insansız hava aracı sistemlerine monte edilip kullanılması diğer klasik fotogrametrik yöntemler ve insansız hava araçlarına monte edilmiş lazer tarayıcı sistemlerine göre gittikçe daha çok popülerleşmektedir. Bu çalışmada insansız hava araçlarına monte edilmiş alıcılardan elde edilen hava fotoğraflarının yeniden düzenlenmesi, işlenmesi ve lokal maksimum yöntemi ile filtrelenmesi sonucunda konifer yapıya sahip ağaçların bulunduğu bir kent ormanındaki ağaçların tekil yüksekliklerinin bulunması gerçekleştirilmiştir. Tüketici sınıfı bir kamera ve 96 cm genişliğe sahip bir İnsansız Hava Aracı (İHA) platformu ile yapılan bir uçuşta 6.41 cm yer örnekleme aralığına sahip hava fotoğrafları çekilmiş, daha sonra bu fotoğraflardan orto-görüntü, sayısal yükseklik modelleri ve nokta bulutu verisi elde edilmiştir. Sayısal yüzey modelinden sayısal arazi modelinin çıkarılması ile elde edilen kanopi yükseklik modeli, piksel tabanlı pencere büyüklüğüne dayalı olarak lokal maksimum ile filtrelenmiştir. Doğruluk analizi için, seçilmiş olan ağaçların yükseklikleri yersel lazer-metre ile ölçülmüştür. Bu ölçümler ile İHA yardımıyla elde edilen ağaç yüksekliklerinin karşılaştırılması sonucunda %94 lük bir korelasyon ve 28 cm'lik karesel ortalama hata elde edilmiştir. Bu çalışma kullanılan yöntemin doğruluğunu desteklemekte ve diğer pahalı yöntemlere göre olumlu ve olumsuz yönleri değerlendirilmektedir.

**Anahtar kelimeler:** İnsansız Hava Araçları, Ağaç Yüksekliği Kestirimi, Fotogrametri, Görüntü İşleme, Lokal Maksimum Filtreleme, Tüketici Sınıfı Kameralar

.../.../20....

## **STATEMENT OF COMPLIANCE WITH ETHICAL PRINCIPLES AND RULES**

I hereby truthfully declare that this thesis is an original work prepared by me; that I have behaved in accordance with the scientific ethical principles and rules throughout the stages of preparation, data collection, analysis and presentation of my work; that I have cited the sources of all the data and information that could be obtained within the scope of the study, and included these sources in the references section; and that this study has been scanned for plagiarism with “scientific plagiarism detection program” used by Anadolu University, and that “it doesn’t have any plagiarism” whatsoever. I also declare that, if a case contrary to my declaration is detected in my work at any time, I hereby express my consent to all the ethical and legal consequences that are involved.

.....  
(Signature)

.....  
(Name-Surname)

This thesis is dedicated to no one, but me...

## ACKNOWLEDGEMENTS

It does not matter how slowly you go, as long as you do not stop. –*Confucius*

I'd like to give my gratitude to my supervisors Asst. Prof. Uğur AVDAN and Assoc. Prof. Tarık TÜRK for their patience and guidance, without them I wouldn't finish this work with utmost success.

I also would like to thank to all who made me what I am today. To my family Ayfer, Kemal and Ekin who bear with me through my whole life, my beloved girlfriend Şebnem for her endless love, my professors, my dearest friends and all...

Although they are in my "dearest friends" category, I'd also like to give my thanks to my friend Mehmet DEMİREL for his graphical genius and unending support, Hüseyin DUMAN for showing me how a researchers' confidence and commitment should be and Ahmet Faruk CİĞER for always cheering me up and being there whenever I needed and lastly Evren GÖLGE who acts like my life coach and supporting me all the way through.

The author would also like to thank Anadolu University of Turkey, Scientific Research Projects department for funding 1407F356 numbered project called "Determination of Tree Heights Using Unmanned Air Vehicles (Eskişehir Urban Forest Example)". Also the author acknowledges Research Institute of Earth and Space Sciences of Anadolu University of Turkey for allowing us the usage of UAV platform and other tools required in the process.

Anıl Can BİRDAL

June 2016

## TABLE OF CONTENTS

	<u>Page</u>
TITLE PAGE .....	i
FINAL APPROVAL FOR THESIS .....	ii
ABSTRACT.....	iii
ÖZET .....	iv
STATEMENT OF COMPLIANCE WITH ETHICAL PRINCIPLES AND RULES .....	v
ACKNOWLEDGEMENTS .....	vii
TABLE OF CONTENTS .....	viii
LIST OF TABLES .....	x
LIST OF FIGURES .....	xi
ABBREVIATIONS.....	xii
1. INTRODUCTION.....	1
1.1. Photogrammetric History and Evolution of Unmanned Aerial Vehicle Systems.....	1
1.2. General Aspects of Unmanned Aerial Vehicles in Photogrammetry and Remote Sensing .....	3
1.3. Research Objectives .....	10
2. LITERATURE SURVEY .....	11
2.1. Previous Works .....	14
2.2. Methodologies for Estimating Tree Heights .....	19
3. MATERIALS AND METHODS .....	22
3.1. Study Workflow .....	22
3.2. Unmanned Aerial Vehicle Platform .....	23
3.3. Study Area and Flight Sessions.....	24
3.4. Field Measurements for Tree Height Validation .....	28
3.5. Generation of Ortho-Images, Digital Surface Models and Point Clouds ....	29



## TABLE OF CONTENTS (Continuing)

3.6. Obtaining Above Ground Level Height .....	30
3.7. Creating the Canopy Height Model.....	31
4. RESULTS AND DISCUSSION .....	33
4.1. Filtering Process with Local Maximum.....	33
4.2. Validation of Estimated and Measured Tree Heights .....	34
4.3. Discussion.....	36
5. CONCLUSIONS .....	39
REFERENCES.....	40
APPENDIX.....	48
RESUME (In Turkish) .....	68
RESUME (In English) .....	70

## LIST OF TABLES

	<u>Page</u>
<b>Table 1.1.</b> Examples of most commonly used UAVs for PaRS applications .....	<b>6</b>
<b>Table 1.2.</b> Commonly used small and medium format visible band cameras for UAV systems .....	<b>7</b>
<b>Table 1.3.</b> Commonly used multispectral cameras for UAV systems .....	<b>8</b>
<b>Table 1.4.</b> Commonly used hyperspectral cameras for UAV systems .....	<b>8</b>
<b>Table 1.5.</b> Commonly used thermal cameras for UAV systems .....	<b>8</b>
<b>Table 1.6.</b> Integrated laser scanner for UAV systems .....	<b>9</b>
<b>Table 1.7.</b> Integrated synthetic aperture radars for UAV systems .....	<b>9</b>
<b>Table 1.8.</b> Unmanned Aerial Vehicle products related to urban forestry uses .....	<b>11</b>

## LIST OF FIGURES

	<u>Page</u>
<b>Figure 1.1.</b> The camera platform below the balloon with the balanced holder of the camera and the ropes .....	2
<b>Figure 1.2.</b> Top left: Aerial photographs of Schlosshotel Kronberg. Bottom left and center: Frankfurt. Right: Pigeons fitted with cameras .....	2
<b>Figure 1.3.</b> UAV platform is being launched on a rampart .....	4
<b>Figure 1.4.</b> UAV platform is being launched with bare hands .....	4
<b>Figure 1.5.</b> From top to bottom, left to right, each picture shows an UAV of each category .....	5
<b>Figure 1.6.</b> An explanation of how LiDAR returns occur .....	13
<b>Figure 3.1.</b> Study workflow .....	21
<b>Figure 3.2.</b> eBee UAV platform with the supplied camera.....	23
<b>Figure 3.3.</b> Study area of Eskişehir Urban Forest .....	25
<b>Figure 3.4.</b> Ortho-image of the test area .....	26
<b>Figure 3.5.</b> UAV and ground control station .....	26
<b>Figure 3.6.</b> Ground measurements were taken with a laser distance meter platform ...	27
<b>Figure 3.7.</b> Left: DSM of the study area. Right: Point cloud of the study area. ....	28
<b>Figure 3.8.</b> AGL height of the test area .....	29
<b>Figure 3.9.</b> Canopy height model of the test area .....	30
<b>Figure 3.10.</b> Individual trees as point features obtained from CHM by using local maximum filter .....	32
<b>Figure 3.11.</b> Ground-measured and algorithm-estimated tree height validation results of 53 test heights .....	33

## ABBREVIATIONS

ALS	: Airborne Laser Scanning
AGL	: Above Ground Level
DMC	: Digital Mapping Camera
GCP	: Ground Control Point
GPS	: Global Positioning System
TIN	: Triangulated Irregular Network
RMSE	: Root Mean Square Error
CHM	: Canopy Height Model
UAV	: Unmanned Air Vehicle
GSD	: Ground Sampling Distance
RGB	: Red, Green, Blue
RTK	: Real Time Kinetic
DTM	: Digital Terrain Model
DEM	: Digital Elevation Model
DSM	: Digital Surface Model
UAV-LiDAR	: Unmanned Air Vehicle-Light Ranging and Detecting
LiDAR	: Light Ranging and Detecting
SfM	: Structure from Notion
MVS	: Multiview Stereo
PaRS	: Photogrammetry and Remote Sensing
MTOW	: Maximum Take-Off Weight
OR	: Operating Range
SAR	: Synthetic Aperture Radars
GNSS	: Global Navigation Satellite Systems
NIR	: Near Infrared
3D	: Three Dimensional
RMSE	: Root Mean Square Error
k-MSN	: k Most Similar Neighbor
EXIF	: Exchangeable Image File Format
USB	: Universal Serial Bus

## **1. INTRODUCTION**

Let them fly and they will create a new market, as Colomina and Molina (2014, p.79) said in their great review of Unmanned Aerial Vehicle (UAV) systems [1], they flew and created a new market. UAV systems have been developing so fast that they are taking classical Photogrammetry and Remote Sensing (PaRS) methods' places by storm. Not only in strict PaRS applications, these systems are used in a variety of fields, such as agricultural and environmental applications [2], intelligence, surveillance and reconnaissance missions [3], aerial monitoring [4], cultural heritage [5], conventional mapping, photogrammetry and also cadastral applications [6]. According to a technical report [7] prepared by MarketsandMarkets, UAV market was valued at USD 10.1 billion in 2015 and is expected to value at USD 14.9 billion in 2020. Regulations all over the world are being prepared for this new kind of aerial technology to be legally used for PaRS applications.

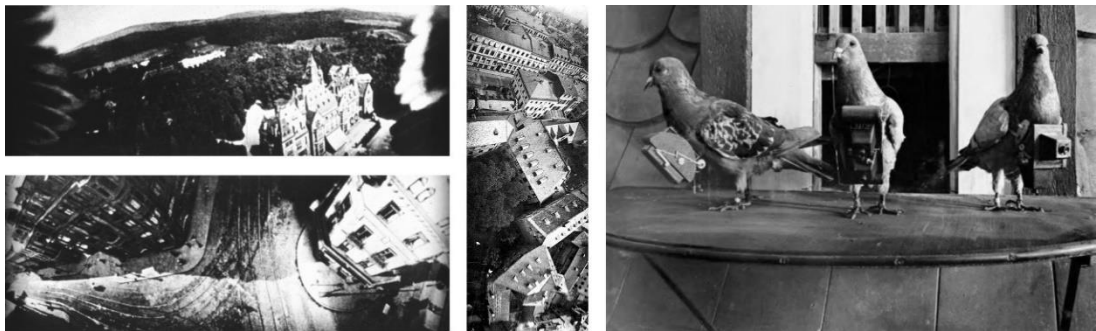
Combined together, computer vision and geomatics technologies have created a new sensation for PaRS and conventional mapping with low altitude and large scales [8-11]. An UAV system usually consists of an unmanned aerial vehicle with related payload, a ground control station for early mission planning and real time navigation and communication link between station and vehicle. Without an onboard pilot, UAVs can maintain a flight pattern above the ground.

### **1.1. Photogrammetric History and Evolution of Unmanned Aerial Vehicle Systems**

For aerial observations mankind used variety of objects including balloons, rockets, planes, kites and even pigeons. Early photogrammetric studies were based on taking photographs from rooftops or hot-air balloons (Fig 1.1). In 1858, French photographer named Gaspard-Félix Tournachon probably took the first photogrammetric photographs recorded in history. E.D Archibald used flying kites as aerial vehicles in 1882 and Alfred Nobel used rockets in 1897 to carry out aerial photography. In 1897, Julius Gustav Neubronner invented probably the most exciting and also the hardest way to take aerial photographs, pigeon photographer method (Fig 1.2) [1].



**Figure 1.1.** *The camera platform below the balloon with the balanced holder of the camera and the ropes [12]*



**Figure 1.2.** *Top left: Aerial photographs of Schlosshotel Kronberg. Bottom left and center: Frankfurt. Right: Pigeons fitted with cameras [13].*

Putting aside rooftop and hot-air manned balloon photography, mankind always relied on an unmanned remote system to take aerial photographs before the first manned aerial platform was invented by Wright brothers. They took the first photographs from a manned aerial system in 1909 [1]. From then on, traditional photogrammetric applications were based on manned aerial platforms with experienced personnel. In late twentieth century with the development of radio-controlled systems, modern UAVs were used for

PaRS applications for the first time. Przybylla and Wester-Ebbinghaus carried out an aerial photographic application with a radio controlled, 3m fixed-wing UAV with an optical camera [1, 14]. Later, same team used a model helicopter to perform a second test with a medium-format camera [1, 15]. These studies were the first time that a UAV platform was used.

## **1.2. General Aspects of Unmanned Aerial Vehicles in Photogrammetry and Remote Sensing**

As it is highlighted in the thesis before, UAV systems consist of unmanned aerial platforms, ground stations and communication links. They are considered as the fundamental components of UAV systems. However there are also other parts such as navigation and imaging sensors, mechanical servos and wireless systems [1].

Without an onboard pilot, UAVs can maintain a level flight pattern above the ground [16, 17]. Launch methods like autonomous, air, hand and mechanical, depends on the size and type of UAV (Fig 1.3, Fig 1.4). The size of the UAV can limit the type of application and the sensor carried onboard. Sensor development within consumer digital camera markets has seen many technological advances resulting in much smaller, affordable and effective sensors for smaller UAV platforms. Technological advances in digital cameras, Global Navigation Satellite Systems (GNSS), and autopilots extensively allowed the use of smaller UAV's as platforms for remote sensing. Autopilots with integrated GNSS aid in flight control, collection of camera positions and also landing, resulting in easy use and autonomous flight. Aerial data collected while UAV is in flight, can be stored directly on the aircraft or camera memory or it can be sent back to ground control station. [16, 18].



**Figure 1.3.** UAV platform is being launched on a rampart [19].



**Figure 1.4.** UAV platform is being launched with bare hands (Top left: Waiting for propeller to work, top right: preparing for launching with hands, bottom left: throwing the UAV forward).

Sensors onboard UAV can produce a wide variety of remotely sensed results like true color UAV ortho-images with higher resolution (1-5 cm) compared to traditional photogrammetric methods, hyperspectral or multi-spectral images, thermal sensed images, Light Detecting and Ranging (LiDAR) sensed point clouds and even full motion videos [16, 20] with real time data gathering.



Eisenbess (2009) [21] provided a valuable report on UAV classification based on many attributes like heavy or light weight platforms, price, weather and wind resistances, powered or non-powered, payload etc. Also in van Blyenburgh's (2013) [22] work, a mass inventory of UAV is presented. Figure 1.5 shows an UAV of each category accordingly.



**Figure 1.5.** From top to bottom, left to right, each picture shows UAVs of each category in [1,22]: AeroVironment, USA-Nano-Hummingbird; Ascending Technologies GmbH, Germany-Falcon 8, CATUAV, Spain-Argos, Swiss UAV, Switzerland-Neo s300; Schiebel Austria-Camcopter S100, MMIST, Canada-Snowgoose; Thales, UK-Watchkeeper; Selex ES, Italy-Nibbio; Insitu Inc., USA-Integrator; General Atomic Aeronautical Systems, USA-Predator A; QinetiQ UK-Zephyr; Lockheed Martin, USA-Morphing UAS.

UAV are classified into many different classes based on their Maximum Take-Off Weights (MTOW), Operating Range (OR), payloads etc. As described in Colomina and Molina (2014, p.81), Medium Range Endurance to Exo-Stratospheric UAV ecosystem is the largest groups that operates at the highest altitude. But these UAVs are commonly are authorized to fly under certain situations decided by military units generally. Next, there

are close-short-medium-range UAVs, and they are characterized as their MTOW is between 150 and 1250 kg and OR between 10 and 70 km. And lastly, there comes nano-micro-mini UAV class which is defined as their MTOW under 30 kg, and operation range less than 10 km. Table 1.1 gives examples of most commonly UAVs used for PaRS applications.

**Table 1.1.** Examples of most commonly used UAVs for PaRS applications [1]

Name	Manufacturer	Weight (kg)	Endurance (h)	Integrated payload (i) or Payload weight (w)
<i>Common fixed-wing unmanned aircraft</i>				
SwingletCAM	SenseFly	0.5	0.5	16 Mpx Red, Green, Blue (RGB) camera (i)
GeoScan101	GeoScan	2	1	24.3 Mpx RGB camera (i)
UX5	Trimble	2.5	0.83	16.1 Mpx MILC RGB camera (i)
Pteryx	FotoMapy	5	2	1 kg w/o batteries (w)
Sirius I	MAVinci	3	0.91	16 Mpx RGB camera (i)
Kahu	Skycam	4	2	Double-head 16 Mpx MILC RGB cameras (i)
<i>Common rotary-wing unmanned aircraft</i>				
Geocopter	IGI	90	2	30 kg (w)
Scout B1-100	Aeroscout	75	1.5	30 kg (w)
R-MAX, type II	Yamaha	100	1	28 kg (w)
<i>Common multi-rotor unmanned aircraft</i>				
Md4-1000	Microdrones	3	1.46	1.2 kg (w)
HT-8-2000	Height-Tech	2.4	0.28	2 kg (w)
Aibot x6	Aibotix	2.4	30	2.5 kg (w)

**Table 1.1.** (Continuing) Examples of most commonly used UAVs for PaRS applications [1]

Falcon 8	Ascending technologies	1.45	0.33	0.75 kg (w)
HexaKopter	MikroKopter	1.2	0.6	1 kg (w)

In UAV based PaRS applications, once the requirements of the application are set, a combination of aerial vehicle and sensing payload should be defined with the best interest for the studies. This combination is not an easy task to be carried out, while considering attributes such as payload's weight, UAV's MTOW, UAV weight, UAV and payload's power requirements etc [1]. Table 1.2 summarizes common small and medium format visible band cameras for UAV systems. Information about multispectral cameras for UAV is provided in Table 1.3. Table 1.4 presents commonly used hyperspectral cameras for UAV systems. Lastly, Table 1.5 describes thermal cameras suitable for UAV mapping.

**Table 1.2.** Commonly used small and medium format visible band cameras for UAV systems [1]  
(Mpx: megapixel, fp: focal plane shutter, ls: leaf shutter, fps: frame per second)

Manufacturer, Model	Format type	Resolution (Mpx)	Size (mm <sup>2</sup> )	Pixel size ( $\mu$ m)	Weight (kg)	Frame Rate (fps)	Speed (s <sup>-1</sup> )
Phase One, iXA 180	MF	CCD sensor 80	53.7 x 40.4	5.2	1.70	0.7	4000 (fp) 1600 (ls)
Trimble, IQ180	MF	CCD sensor 80	53.7 x 40.4	5.2	1.50	-	1000 (ls)
Hasselblad, H4D-60	MF	CCD 60	53.7 x 40.4	6.0	1.80	0.7	800 (ls)
Sony, NEX-7	SF	CMOS 24.3	23.5 x 15.6	3.9	0.35	2.3	4000 (fp)
Ricoh, GXR A16	SF	CMOS 16.2	23.6 x 15.7	4.8	0.35	3	3200 (fp)

**Table 1.3.** Commonly used multispectral cameras for UAV systems [1]

Manufacturer, Model	Resolution (Mpx)	Size (mm <sup>2</sup> )	Pixel size (μm)	Weight (kg)	Spectral range (nm)
Tetracam, MiniMCA-6	CMOS 1.3	6.66 x 5.32	5.2 x 5.2	0.7	450-1050
Quest Innovations, Condor-5 UAV-285	CCD 1.4	10.2 x 8.3	7.5 x 8.1	0.8	400-1000

**Table 1.4.** Commonly used hyperspectral cameras for UAV systems [1]

Manufacturer, Model	Resolution (Mpx)	Size (mm <sup>2</sup> )	Pixel size (μm)	Weight (kg)	Spectral range (nm)	Spectral bands and resolution
Rikola Ltd., Hyperspectral Camera	CMOS	5.6 x 5.6	5.5	0.6	500 - 900	40, 10 nm
Headwall Photonics, Micro-Hyperspec X-series NIR	InGaAs	9.6 x 9.6	30	1.025	900 - 1700	62, 12.9 nm

**Table 1.5.** Commonly used thermal cameras for UAV systems [1] (mK: millikelvin)

Manufacturer, Model	Resolution (Mpx)	Size (mm <sup>2</sup> )	Pixel size (μm)	Weight (kg)	Spectral range (μm)	Thermal sensitivity (mK)
FLIR, TAU 2 640	Uncooled VOx Microbolometer, 640 x 512	10.8 x 8.7	17	0.07	7.5 – 13.5	≤ 50
Thermoteknix Systems Ltd., Miricle 307K-25	Amorphous Silicon, 640 x 480	16 x 12.8	25	0.105	8 - 12	≤ 50

Not only cameras are applied to UAV for PaRS applications. There are also LiDAR scanners [1, 23, 24] and Synthetic Aperture Radars (SAR) [1, 25-27] suitable for UAV, but still remains challenging in most ways due to cost, size, flight dynamics etc. Table 1.6 provides some information about successfully integrated LiDAR systems onboard UAVs and Table 1.7 describes successfully integrated SAR systems onboard UAVs.

**Table 1.6.** *Integrated laser scanner for UAV systems [1] (A: automotive, MM: terrestrial mobile mapping, H: hydrography, deg: degree, app: application)*

Manufacturer, Model	Scanning Pattern	Range (m)	Weight (kg)	Angular res. (deg)	FOV (deg)	Laser class and $\lambda$ (nm)	Frequency (kp/s)	App.
Ibeo Automotive Systems, IBEO LUX	4 Scanning Parallel lines	200	1	(H) 0.125 (V) 0.8	(H) 110 (V) 3.2	Class A, 905	22	A
Velodyne, HDL-32E	32 Laser/detector Pairs	100	2	(H) – (V) 1.33	360 (V) 41	Class A, 905	700	MM
RIEGL, VQ-820-GU	1 Scanning Line	$\geq 1000$	-	(H) 0.01 (V) N/A	60 (V) N/A	Class 3B, 532	200	H

**Table 1.7.** *Integrated synthetic aperture radars for UAV systems [1] (NanoSAR B weight doesn't account for antenna and Inertial Measurement Unit)*

Manufacturer, Model	Spectral Bands	Weight (kg)	Transmitted power (W)	Resolution (m)
IMSAR, NanoSAR B	X and Ku	1.58	1	Between 0.3 and 5
Fraunhofer FHR, MIRANDA	W	-	0.1	0.15
NASA JPL, UAVSAR	L	200	2000	2
SELEX Galileo, PicoSAR	X	10	-	1

### **1.3. Research Objectives**

In this study, a low-cost UAV system is used to derive tree heights and crowns. A consumer-grade RGB camera on a lightweight UAV (< 0.70 kg) was used to generate ortho-images, which were then used to construct a DSM and DTM of the study area. By subtracting the DSM from the DTM, real height model (which contains the heights based on the ground surface), known as CHM, is used to be filtered with the local maximum filter algorithm to obtain the individual crown points and heights of the trees. Afterwards, tree heights were measured in the field with a laser distance meter and compared to tree heights estimated by a local maximum filter.

## 2. LITERATURE SURVEY

Mini-UAV platforms are suited well for urban forest applications. UAV generated products for urban forestry can be used in many ways (Table 1.8). A spatial tree inventory is needed when it comes to understanding how people manages urban forests and surrounding areas. Urban forest inventories include information like species, diameter, condition, maintenance needs, location, height, growing class etc. which requires an update in specified time intervals. An indirect benefit of inventory analysis with the UAV platform is the collection and archiving of aerial imagery for future temporal comparison. To complete spatiotemporal analysis to detect changes over time, small UAV applications presents an affordable repeatability of acquiring aerial imageries. Multi-temporal data collected by the UAV platform will provide effective comparisons to understand landscape change and monitoring [28]. Inventory and spatial comparisons will provide valuable information of urban forest structure and that will lead to more effective management decisions [16].

**Table 1.8.** UAV products related to urban forestry uses [16]

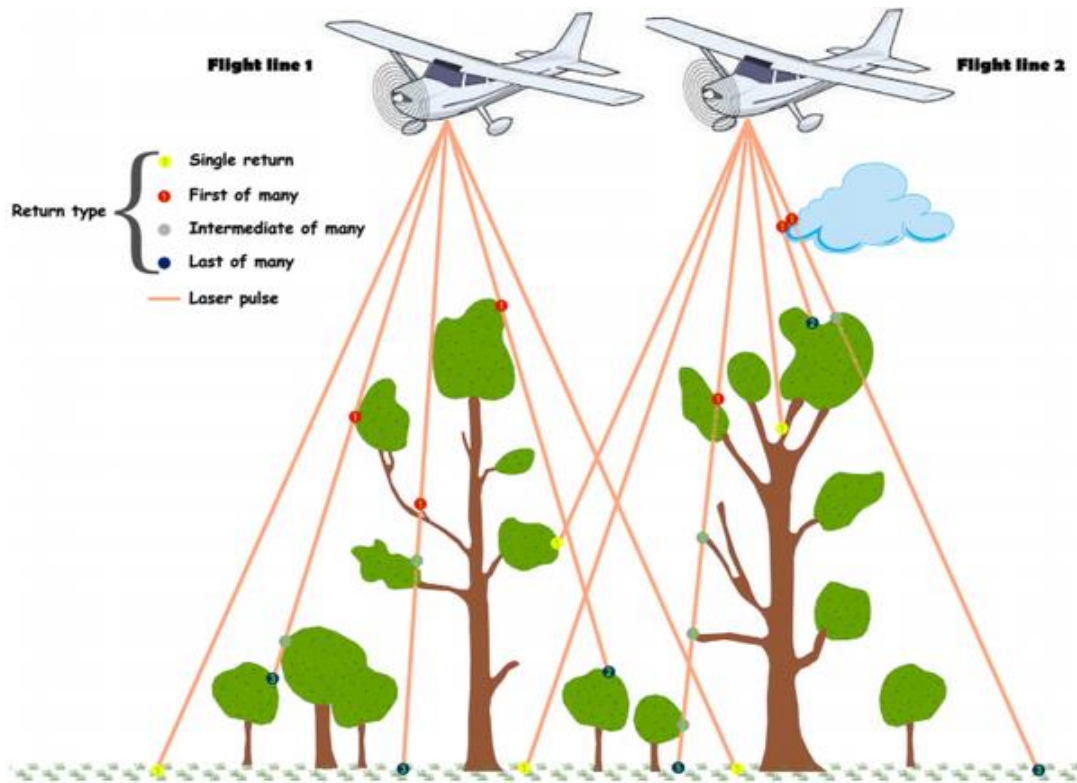
UAV Products	Urban Forestry Uses
Color aerial photography	Land cover/use mapping
	Historical documentation
	Tree inventory
	Vegetation analysis (crown density)
	Temporal comparison
	Planning
	Maintenance
	Planting
	Wildlife corridors
	Landscape fragmentation
Near Infrared (NIR) photography	Vegetation analysis
	Tree monitoring
	Vegetation health monitoring

**Table 1.8.** (Continuing) *UAV Products related to urban forestry uses [16]*

LiDAR	Tree heights
	Topographic analysis
	Watershed analysis
	Infrastructure analysis
	Soil moisture
	Forest structure
Digital Elevation Model (DEM)	Three Dimensional (3D) Modeling
	Contours
	Road/trail desing
	Slope/aspect
	Elevation
Thermal Imaging	Vegetation analysis
	Insect/disease monitoring
	Drought sensitivity

Calculating the canopy and individual tree heights of a forest with remote sensing techniques is highly accurate and reduces time and cost compared to traditional approaches. Airborne LiDAR is the most commonly used system for deriving metrics from a forest area. A summary of how LiDAR returns occur is presented in Fig 1.6. There have been several studies on the use of airborne LiDAR platforms in forest areas that show accurate results [29, 30] with the use of UAV-LiDAR platforms [31, 32] and even with spaceborne LiDAR platforms [33]. However, despite these highly accurate results, short flight sessions and the high cost of these surveys with experienced personnel prevent continuous studies [23, 34]. Imagery obtained from UAVs can be used to obtain point clouds similar to LiDAR point clouds that results in creating DEM, DTM and CHM products [16, 35]. There have also been studies with the satellite images [36, 37] based on forest structure and the spatial resolution of the satellite images; the results are less precise but useful for large areas.





**Figure 1.6.** An explanation of how LiDAR returns occur [38]

In recent years, UAVs equipped with consumer-grade cameras have provided the most convenient approaches for inventory, monitoring, and modeling applications [33, 34]. Lightweight UAV platforms (< 2 kg) can fly longer than Airborne LiDAR and UAV-LiDAR platforms, which helps to reduce survey costs.

In order to estimate individual tree metrics, high resolution DEMs and photogrammetric point clouds must be generated to create CHMs. With photogrammetric point clouds, virtual tree models can be generated [39]. Classification of these point clouds based on their geometric characteristics can prove useful in avoiding detection errors and the interpolation of the terrain beneath the forest structures [40]. However, generating only a few points from the ground surface in dense forest may be problematic when interpolating the terrain [23]. Therefore forest structure types become significant when it comes to detecting tree crowns or real tree heights [41].

Miniaturized UAV payloads, including consumer-grade cameras, GNSS, and embedded computer systems provide poorer quality images with geometrical deformations, as compared to traditional metric systems used on airborne platforms [34, 42]. Several methodologies like Structure-from-motion (SfM) and Multiview-stereo

(MVS) should be performed to correct for these issues [34,43-48]. Traditionally, airborne photogrammetric acquisition of images has been used to obtain canopy heights [49,50] with onboard Digital Mapping Cameras (DMC). These surveys produce promising data, but with high time and cost requirements.

## **2.1. Previous Works**

All the related literature publications are examined carefully in order to select the best method to obtain tree heights in a human-made forestry area. Some of the researchers that are listed below had the advantage of studying in tree fields that are created for research purposes. Some of them had spacing between trees 2 to 10 meters so that main objects of the study can be identified and modeled easily without merging or blending with other trees surrounding. Some of them studied within natural forest areas but most of their aim was not to single out individual trees but classifying them in a whole manner.

These publications can prove that tree crown detection and height estimation is solely based on the characteristics of individual trees and forest areas. Longer spacing between the trees can solve the problem, but no researcher can expect that natural forest areas would form according to this idea.

Colomina et al. [1] provided a great review of all unmanned aerial systems used till February 2014 for photogrammetry and remote sensing. They discussed UAV platforms, all kinds of sensors onboard UAV systems and also their application to a variety of fields. Also Remondino et al. [48] discussed the current status and future perspectives of UAV photogrammetry till 2011 September. They presented UAV image processing methods for photogrammetric application, mapping and 3D modeling.

Küng et al. [43] discussed the accuracy of automatic photogrammetric processes of ultra-light UAV imageries with several datasets also analyzed their accuracies. They proved that the accuracy highly is dependent on flying height of the UAV platform. A comparison of the robust and fully automated process of UAV image processing systems and traditional photogrammetric processing systems in their publication. Also Vallet et al. [46] provided a photogrammetric performance evaluation publication for Swinglet UAV from Sensefly, Parrot Company.

Popescu et al. [51] used airborne LiDAR technology to estimate tree heights in their study. High density and small-footprint LiDAR data was acquired from coniferous,

deciduous and some other mixed stands in order to justify the effects of tree types. Not only the used airborne LiDAR to estimate the tree heights with filtering methods, but they also used ground truth data to investigate how ground measurements can help to the processing stage. As a result, they achieved 85 and 90% correlation with two different methods. They concluded with stating the variable window size algorithm performed better for estimating the tree heights of dominant and co-dominant trees.

Gougeon et al. [37] applied tree crown approach to Ikonos images in a coniferous plantation area. They used two base Ikonos images with 1 m (panchromatic) and 4 m (multispectral) spatial resolutions and also used same approach in winter and summer seasons. Panchromatic images were resampled and smoothed using a 3x3 kernel mean filter. In study area, trees were counted to estimate the accuracy of tree crown delineation. Also, on smoothed images, a local maxima was used with a 3x3 sized window for comparison. Individual tree crown and local maxima approach were off from ground validation data with a percentage of 15 for both season. They performed an individual tree crown based classification by using multispectral Ikonos images to generate an overall accuracy test. With the classification results compared to trees with known-species, accuracy was 59 percent. They claimed confusion with classification results were mostly within white and red spruces.

Packalên et al. [52] used k Most Similar Neighbor (k-MSN) method on airborne laser scanning data to predict forest variables like volume, stem number, basal area, basal area median diameter and tree height. They used a non-parametric k-MSN method to a combination of airborne laser scanning data and aerial photographs to predict the variables for Scots pine, Norway spruce and deciduous other tree species. They used the vegetation returns of the laser beams to predict tree heights. They claimed this method worked best for Scots pine and Norway spruces than other deciduous trees, also better than related field inventory ground measurements.

Monnet et al. [53] investigated tree top detection algorithm with several parameter combinations to evaluate its performance. Their algorithm consisted of digital elevation model reconstruction, Gaussian smoothing, morphological filtering and local maxima selection and extraction. Detection rates are achieved over 42.9% with 4.1% false positives for Silver fir, Norway spruce and European beeches. They used the optimal settings in one study area and tested it in the other areas. They claimed that optimized

parameters are dependent on the laser data, mostly point density and also forest structures and species.

Vauhkonen et al. [41] used airborne laser scanning data to derive height, intensity and alpha shape metrics like diameter at breast height, stem volume etc. They tested nearest neighbor imputation by k-MSN method and also used the Random Forest method for the estimation of species, diameter at breast, height and stem volume. Random Forest method proved valuable asset to classify Scots pine, Norway spruce and deciduous trees, with handling 1846 predictors without the need to reduce them. They achieved 13%, 3% and 31% root mean square errors for diameter at breast, height and volume attributes respectively.

A comparison between individual tree and height detection algorithms has been made by Vauhkonen et al. [54]. Their results showed that forest structure, in particular tree density and clustering affects the performance of all the algorithm regardless, also training with local data helped to improve the results. They provided a good summary of all algorithms used to derive tree metrics to guide the user to choose the according method to their interest.

Wallace et al. [23] discussed the development of UAV-LiDAR systems with application to forest inventories and also modified a processing workflow to improve the horizontal accuracy of the point cloud by including a GNSS, an inertial measurement unit and a high definition video camera from 0.61m to 0.34m as root mean square error. With higher density data such as 62 point per m<sup>2</sup>, they achieved root mean square error of 0.15m. They claimed horizontal accuracy of point data was mostly affected due to including a video camera in the system. Wallace et al. [31, 32] also discussed the current tree detection algorithms with UAV-LiDAR systems.

Wallerman et al. [49] investigated the usage of digital elevation models acquired from aerial imagery taken with digital mapping cameras onboard photogrammetric suited planes (4800 m above ground, 60% stereo overlap in along-track and 30% in across-track). They applied a single tree modeling approach similar to individual tree crown method commonly used in airborne laser scanning. A simplified individual tree crown method was used to estimate tree height and their root mean square error was 34% (of the true mean maximum tree height). They provided an alternative to LiDAR approach to forest inventories.

Waser et al. [50] studied high resolution DSM from infrared colored images to obtain shrub/tree cover in open mire lands. Two different types of forest masks were gathered from the DSM with a multi-resolution segmentation and a fuzzy classification. They claimed that for future mire protection, modeling small shrubs and trees with high accuracy by using this technique would prove great value and also eliminate the question of forest/non-forest area.

Waser et al. [55] also studied classification of tree species in different forest ecosystems with images taken with line-scanning sensor airborne digital sensor 40 (ADS40) and aerial row camera (RS30) which provided overlap up to 90% and higher radiometric resolution. Within two study areas, 517 trees had been visited in the field and detected in the images were evaluated. Classification results provided an overall accuracy between 0.76 and 0.83 while classifying dominant tree species. Lower accuracies were obtained for small and non-dominant tree species in study areas. Their study shows the potential of multi-resolution image segmentation applied on CHMs for forest inventories.

Zarco-Tejada et al. [34] investigated the pixel resolution matter for UAV imagery used to obtain tree heights. They used a 2m wingspan fixed-wing platform with 5.8kg take-off weight and obtained Very High Resolution (VHR) imagery to generate orthomosaics and DSMs. Their study yielded an overall root mean square error for tree heights as 35 cm. They also claimed that pixel resolution lower than 35 cm degraded the accuracy of the application. Zarco-Tejada et al. [56] studied leaf carotenoid content estimation, also [36] water stress detection of canopy with micro-hyperspectral imager and a thermal camera.

Fritz et al. [47] compared UAV based photogrammetric point clouds to terrestrial laser scanning with application of tree stem mapping. Data collection were done in leaf-off state in April 2013 which is a big advantage that can eliminate the negative effects of overgrowth foliage. UAV platform had a Panasonic G3 consumer grade camera with 16.6 megapixel sensor which took over 1000 images with a tilt angle of 45°. The results were compared to data obtained with terrestrial laser scanner point cloud. They claimed that two point clouds surprisingly correlated well with each other with a Pearson's correlation coefficient of 0.696.

Takahashi et al. [36] used remote sensed images from Panchromatic Remote-sensing Instrument for Stereo Mapping (PRISM) onboard Advanced Land Observing Satellite (ALOS). They extracted the digital terrain model from digital surface model in

order to obtain CHM of the study area. Over 1000 trees were individually ground measured with an aim to be compared to resulting data obtained from the satellite images. They claimed there was positive correlation between two data sets and also the next part of the study will be in natural forest areas with higher trees.

Chen et al. [57] used watershed segmentation method on CHMs in order to locate tree heights in a savanna woodland. They used small footprint LiDAR data point cloud to create CHMs. The treetops were located by searching a local maxima in canopy maxima model. They combined variable parameters in order to get the best results to isolate individual trees. Their results showed that absolute accuracy of the tree isolation was 64.1%.

Kattenborn et al. [40] used UAV based point clouds to detect single palm trees. They provided the algorithm parameters with ground-based measurements in order to obtain the best results. They also evaluated the pixel resolution matter like Zarco-Tejada et al. [44] with two flight campaigns at 70 and 100m. The point clouds were classified as three classes of palm (1), other vegetation (2) and ground (3). Their results provided a good amount of 86.1% for the entire study area and also 98.2% for dense growing palm stands.

Sperlich et al. [39] used UAV based point clouds data with LiDAR data processing software and evaluated the potential of UAV based photogrammetric point clouds for single tree detection and height derivation. As reference data, they used terrestrial laser scanning point cloud data. Their results clearly showed that tree detection accuracy were dependent of reference tree height and tree density. They claimed that unreliable tree crown formations could results in detecting more than one crowns belonging to an individual tree.

The approach used in this thesis is similar to “Adaptive filtering based on CHM height values” method which will be explained later in “Materials and Methods” chapter. Advantages of this study would clearly be the ease of data acquisition and fully-automated processing stage. Raster reconstruction part is the most complex and user-defined stage of this process, because it’s highly dependent on training data which are Above Ground Level (AGL) height measurements and positions of these trees.

## 2.2. Methodologies for Estimating Tree Heights

There are several methodologies for single-tree detections. A comparative testing between some of these LiDAR data based methods can be found in Vauhkonen et al.'s [54] work. Their results showed that forest structure deeply affects the performance of all algorithms. Tree detection success was especially based on density and clustering of trees in study areas. These algorithms significantly differed from each other particularly in tree detection rather than height estimation. In this study, point clouds obtained from UAV aerial imagery will be processed with LiDAR methods used to obtain individual tree heights in a forest area. A summary of the applied methods are given below. Kaartinen and Hyypä's (2008) [58] report gives far more detailed information about wider range of algorithms used for this type of studies.

Cluster formation using modified k-means approach: By using ground based training data, a Euclidian distance criteria is used to eliminate unwanted local maximums. Wanted local maximums were pretended as seed points. According to these points, a k-means vector quantization algorithm is used to cluster the point data. Training data based height reduction factor is used to lower the bias to improve the clustering of similar objects [53, 59].

A voxel layer single tree modelling algorithm: This algorithm works on density images which are calculated from consecutive height layers that are extracted from point data projected into a voxel space. These images are then traced with a hierarchical morphological algorithm from top to down, assuming there occurs a tree crown when higher amounts of points are traced [53, 60].

Adaptive segmentation based on Poisson forest stand model: A pit-filling algorithm for the CHM and then a low-pass filter with a binominal kernel is used based on the expected nearest neighbor distances between trees. According to each ground training data CHMs are interpolated to various resolutions suitable for extracting smallest tree crown in forest areas [53, 61, 62].

Local maxima detection with residual height adjustment: The first return of point cloud data is interpolated into a DSM with various resolutions depending on the training data. This DSM is smoothed by running a 3x3 Gaussian filter by a number of times, assuming the DSM is pit-free eventually. First return heights of the DSM is calculated using a percentile residual height distribution. The window size, the number of Gaussian

runs and the residual height percentile adjustment is set specifically for each study areas, based on the ground measured tree height and positions [53, 63].

Segmentation based on geometric tree crown models: Calculating the correlation between the point cloud data height and a geometric tree crown model that is placed at the center of a pixel is the basis of this algorithm. An image created with this correlation is used in tree detection with marking each raster cell with a non-zero CHM value and a positive correlation value as seed points. Until a local maximum is found where a seed doesn't have a high correlation with neighbor seeds, these seed points are updated to neighbor cell that has highest correlation. The final seed is characterized as tree crown segment [50, 64-66].

Adaptive filtering based on CHM height values: In this method, CHMs are low-pass filtered using Gaussian kernels. After the filter process, CHMs are interpolated into a grid of desired value i.e. 0.5m by using the maximum of the first return in the related grid. The empty cells in the CHM are filled by filtering the CHM with a defined window size by taking the average of pixels within the window. This algorithm needs a pre requirement of defining window sizes and height classes in order to produce results [53, 67].

The methods mentioned above uses two kinds of input data which are point clouds and CHMs. Also, these methods are highly dependent on training data based on ground measurements. Results of these methods can be significantly improved with better training data as it is obtained with better ground measurement tools [50].

The approach used in this thesis is similar to “Adaptive filtering based on CHM height values” method. Point cloud derived from aerial images will be the base data for this study. After point clouds are obtained, a raster reconstruction stage comes next. In this stage, highest point heights, which are assumed to be first returns of laser pulses, are diffused into pre-defined pixel sizes which are highly dependent on training data and calculated from them. A pit-free CHM is the best raster data can be used for this approach, so a filter is used to fill the empty pixels, which have no point cloud data at all, with the average heights of the neighbor pixels. Highest returns from user-defined pixel sizes will be tagged as tree tops or crown respectively. These tags will be checked up as if they are the highest points can be identified as tree tops with a circular window defined according to the height of trees. If any higher point is tagged while the circular window is being searched, the original point would be untagged as tree top. User-defined pixel size is



based on how many pixels a tree would fit in i.e. with 0.5m x 0.5m pixel size, we can assume a tree can fit in a 3x3 pixel size which would mean the foliage of the tree is 3x3 pixels wide (1.5m x 1.5m).

### 3. MATERIALS AND METHODS

#### 3.1. Study Workflow

Forestry work with UAV platforms started off in the 2000s with model planes and helicopters [46, 68, 69]. Recently they have been used with consumer-grade cameras and low-cost systems in order to make surveys more efficient. Workflow used in this thesis on how to generate individual tree heights and positions is shown in Figure 3.1. This workflow is semi-automated. Ground Control Point (GCP) measurements, ground based tree height and position measurements are obtained through manual labor. Reconstruction of DSM and CHM is highly dependent on local training data, therefore they also require user interactions.

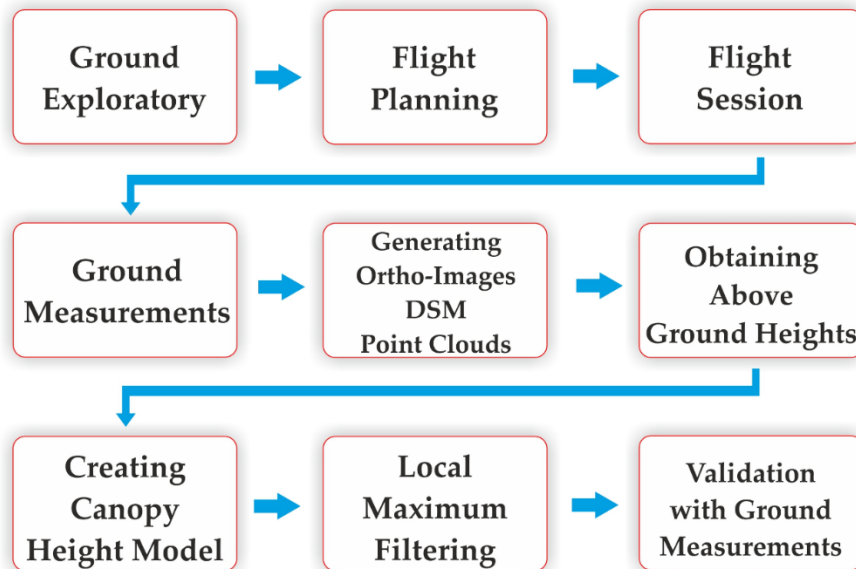


Figure 3.1. Study workflow

In “Ground Exploratory” stage, which took about half a day, a take-off and a landing area has been evaluated to reduce the landing and take-off damages might be caused to UAV platform. Also, types of trees were identified to understand their growing classes and foliage structure. In “Flight Planning” stage, preliminary parameters of UAV flight, which are explained later in “Study Area and Flight Session” section, were evaluated based on area covered by the test area, wind velocity, atmospheric conditions

etc. During “Flight Session” stage, only 28 minutes were spent for flying the UAV and GCP measurements took approximately 1 hour, which made preliminary field survey took less than 1.5 hour in total.

“Ground Measurements” stage was the most tiring and time-consuming part of this study. In total, 91 trees were measured. Trees were selected for measurement, based on how clear they can be identified from nadir imagery. Only 53 of these trees were located in the test area. A whole day was spent for this stage with only one person, including measuring and recording in the field with pen and paper and also transferring data to computer environment. In “Generating Ortho-Images, DSM and Point Clouds” stage, a fully automated process was conducted. Details of this part is explained in the corresponding section. This stage only took only half a day with a high end computer. Performance of processing computer may change time-consume of this part. “Obtaining Above Ground Measurement” stage was associated with reconstruction of the point cloud data to obtain AGL height of the test area. This stage only took about 10 minutes, due to having a small test area with point count lower than one million.

In “Creating Canopy Height Model” stage, a raster was created based on point cloud data which will be named as CHM. Ground training data were used for this stage in a significant manner. “Local Maximum Filtering” part was associated with filtering process of the CHM created on the previous section. This stage only took about 10 minutes, but based on the capacity of the data, time spent for the stage may rise. “Validation with Ground Measurements” stage was the second most time-consuming part of this study, as it involves matching ground measured and algorithm-obtained tree heights not only by locations but also in paper sheet process. Matched heights were then analyzed statistically to understand the relation between them. This stage took approximately one day.

In total, less than 3 days were spent to obtain individual tree height of the test area. This time-consume may depend on the area covered by the study area, performance of the processing computer and also the experience of the personnel.

### **3.2. Unmanned Aerial Vehicle Platform**

A lightweight UAV platform (eBee), which is developed by senseFly, a Parrot company, was used throughout this study. The eBee is a fixed-wing UAV that weighs less than 0.70 kg with the camera and has a wingspan of 96 cm (Figure 3.2). Its cruising

speed ranges from 40 to 90 km/h, which makes it suitable for mapping up to 12 km<sup>2</sup> (1200 ha) with a maximum flight time of 50 minutes. Technical specifications of eBee can be found in Appendix 4. The camera was a Canon IXUS 127 HS with a 4608 x 3456 pixel detector that captured images at f/2.7 and 1/2000 s. Technical specifications of the camera can be found in Appendix 2. According to Directorate of General of Civil Aviation regulations about UAV's usage in Turkey (which was accessed on August, 2016), UAV used in this study is classified as İHA0. These classes are identified based on MTOWs of the UAVs. İHA0 limits the MTOW of the UAV between 0,5-4 kg, İHA1 limits it between 4-25 kg, İHA2 limits it between 25-150 kg, while İHA3 classifies UAVs over 150 kg MTOW.



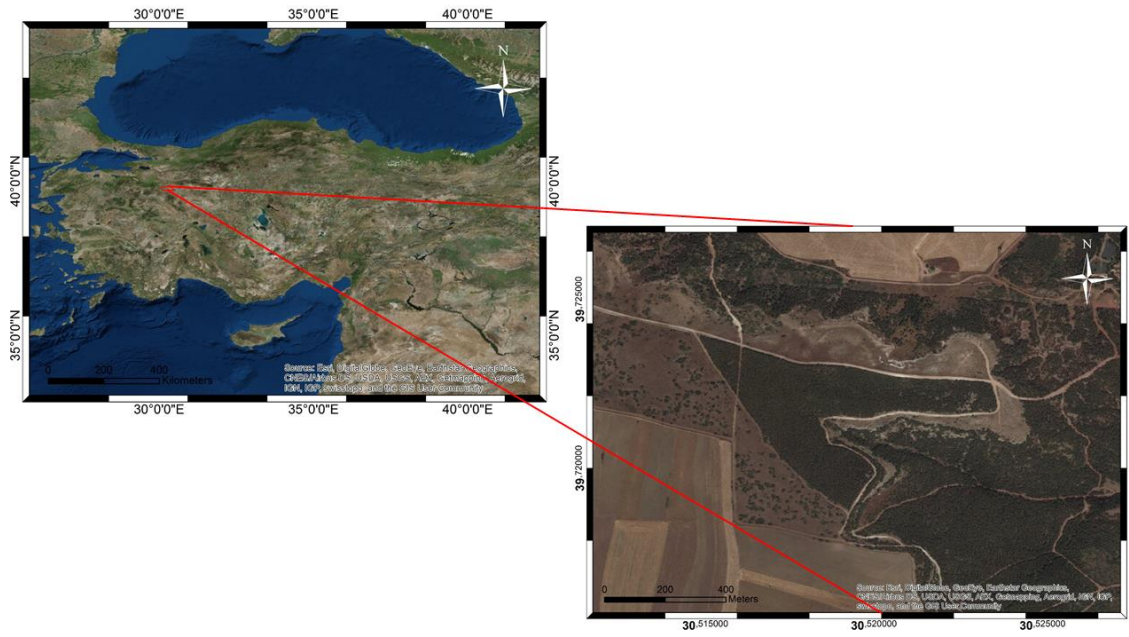
**Figure 3.2.** *eBee UAV platform with the supplied camera.*

### **3.3. Study Area and Flight Session**

The study area was a human-made forest called the Urban Forest of Eskişehir City, Turkey (Fig 3.3). This forest area has a recreation and hiking areas which are used frequently by the local people. A portion of the forest is planted to be used as fire fuel when they are grown into eligible sizes for pruning. The forest consists of mostly black and scots pines which were planted in 1960 and covers approximately 15 ha, of which we studied roughly 1 ha. Test area is a small part of the forest to the south. The main reason behind using a small test area is to work on a seamlessly ortho-image. Wind resistance of mini UAVs are not considered at their best, so in our image acquisition stage, some aerial

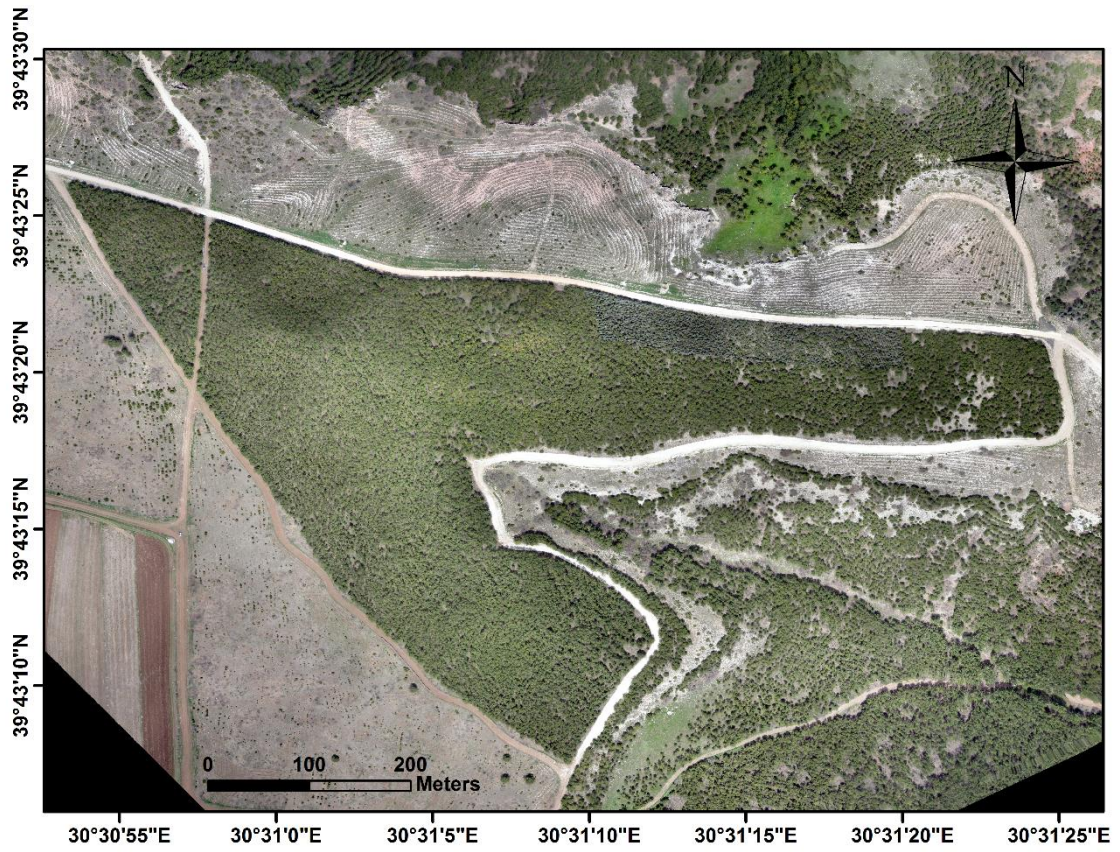
images were not taken in smooth conditions. Therefore test area is selected based on the seamless parts of the ortho-image of the study area. Flight sessions' day and time were selected based on the low wind speed occurring over the study area. Also, military services were alerted about the time of the flight was going to occur to prevent any crashes or panics if the UAV would be considered as unidentified flying objects. During the 28-minute flight, 133 images (Figure 3.4a) were taken from 150 m AGL with 6.41 cm Ground Sampling Distance (GSD). High overlapping parameters were used between each image, %80 forward lap and %70 side lap respectively. Based on Zarco-Tejada et al.'s work in 2014 GSD has been selected around 6 cm in order to get the best results for the CHM. They tried reconstructing the CHM of their study area in order to get the best GSD related to their study purpose. Aerial imagery were stored on a memory card embedded in the supplied camera. Communication with ground control unit was provided with using 2.4 GHz radio link and a Universal Serial Bus (USB) computer connection (Fig 3.5). A hand launch system was used at the beginning of flight which was fully automated from taking off to landing. Six three-dimensional Ground Control Points (GCP) were used, obtained via GNSS through Real Time Kinetic (RTK) technique. Technical specifications of the GNSS used in this study can be found in Appendix 5. The UAV operated with high effectiveness and provided high resolution aerial images. Based on these images, ortho-images (Figure 3.4b), DSMs, and point clouds were produced. For visualization purposes, ArcGIS software developed by Environmental System Research Institute (ESRI) [70] was used.





**Figure 3.3.** Study area of Eskişehir Urban Forest





**Figure 3.4.** *Ortho-image of the test area*



**Figure 3.5.** *UAV and ground control station*



### 3.4. Field Measurements for Tree Height Validation

In total, 53 trees were selected for field measurements to validate the heights estimated from imagery. Measurements were taken with a laser distance meter platform ( $\pm 1$  mm) (Figure 3.6) and the trees' positions were recorded with GNSS. Technical specifications of the laser distance meter can be found in Appendix 3. The reason a laser distance meter was used is because of its cost and working speed. Although there are more accurate devices like laser scanners or total stations theodolites, the purpose of this study is to prove the low cost of this methodology thus making laser distance meter more suitable for this study. Ground measurements were made the day after the flight. Measurements were made from the bottom, where the stem base meets the ground, to the tree top, which rises above other branches. In dense forest areas, a ladder set against another tree was used to spot the crown of the trees if it could not be seen from the ground. Then the laser distance meter was placed on the ground with a visible point of view to the tree top before measuring. Collected heights were recorded with pen and paper. Because the GNSS did not work in areas with dense foliage, trees selected for validation were near clearings, which could also be more easily measured. The GNSS recordings were not the precise position of each tree, considering the algorithm processed positions couldn't match with locations of tree bodies (stems) due to detecting maximum canopy height point's position, but they were easily paired with the correct tree in the processing stage.

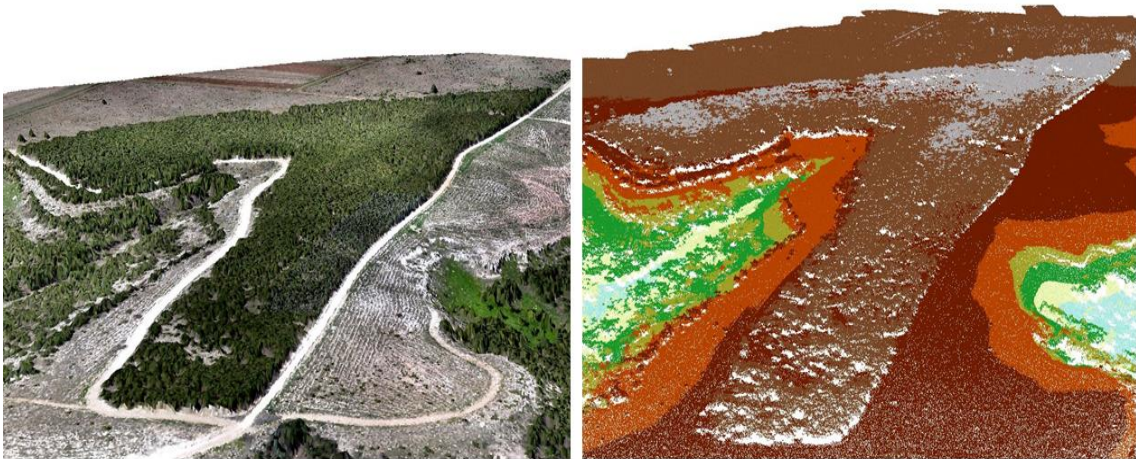


**Figure 3.6.** *Ground measurements were taken with a laser distance meter platform*



### **3.5. Generation of Ortho-images, Digital Surface Models and Point Clouds**

Image processing started with geotagging flight information and camera parameters to each image accordingly. Geotagging is a process of adding geographical identity to all the images collected from the flight. These metadata adds related information to Exchangeable Image File Format (EXIF) header that contains coordinates and parameters of the camera. Ground control information based on GCPs were created as a text file. This text file contained the names and coordinates for each GCP. In all images, an analysis was made to determine if there was any GCPs present, later to be selected to match with related pixel's x,y values. Six GCPs were used with a mean error of 0.041 m. In a fully-automated process, all 133 images were calibrated. A total of 1752,447 key points were used for the bundle block adjustment with 58,7230 3D points. The mean reprojection error of the adjustment was 0.3 pixels, or approximately 2 cm. Postflight Terra 3D, powered by Pix4D which is developed by Swiss Federal Institute of Technology [71] was used in the fully-automated process and the quality report of the process can be found in Appendix 1. This software is based on automatically finding thousands of common points between images. Each characteristic point found in an image is called a keypoint. When 2 keypoints on 2 different images are found to be the same, they are matched keypoints. Each group of correctly matched keypoints will generate one 3D point. The point cloud is a set of 3D points that reconstruct the model. The X, Y, Z position and the color information is stored for each point of the point cloud. The resulting DSM and point cloud data are shown in Figure 3.7. Detailed information can be found about creating point clouds from aerial imageries with SfM in Schönberger et al. (2014)'s [72] work.



**Figure 3.7.** *Left: DSM of the study area. Right: Point cloud of the study area*

### **3.6. Obtaining Above Ground Level Height**

In order to obtain the AGL heights of the trees, we used the point cloud data to interpolate the terrain beneath the forest structure. First, point cloud data were classified as ground points or non-ground points. Ground points were then triangulated into a triangulated irregular network (TIN). The most important part of interpolating the terrain is how many points can be gathered under the foliage. Fewer and less accurate point cloud data would cause problems in accuracy. Large overlapping areas of the images help create more accurate and denser point clouds. Average density of point cloud data used for this study was roughly 40 points per  $\text{m}^3$ . LAStools software, developed by Rapidlosso GmbH [73] was used in this process. There were no trees over 8m height, so a threshold of 8m maximum height was used in order to eliminate abnormalities like bird hits or other noises. Based on the TIN, each point's height was calculated (Figure 3.8).

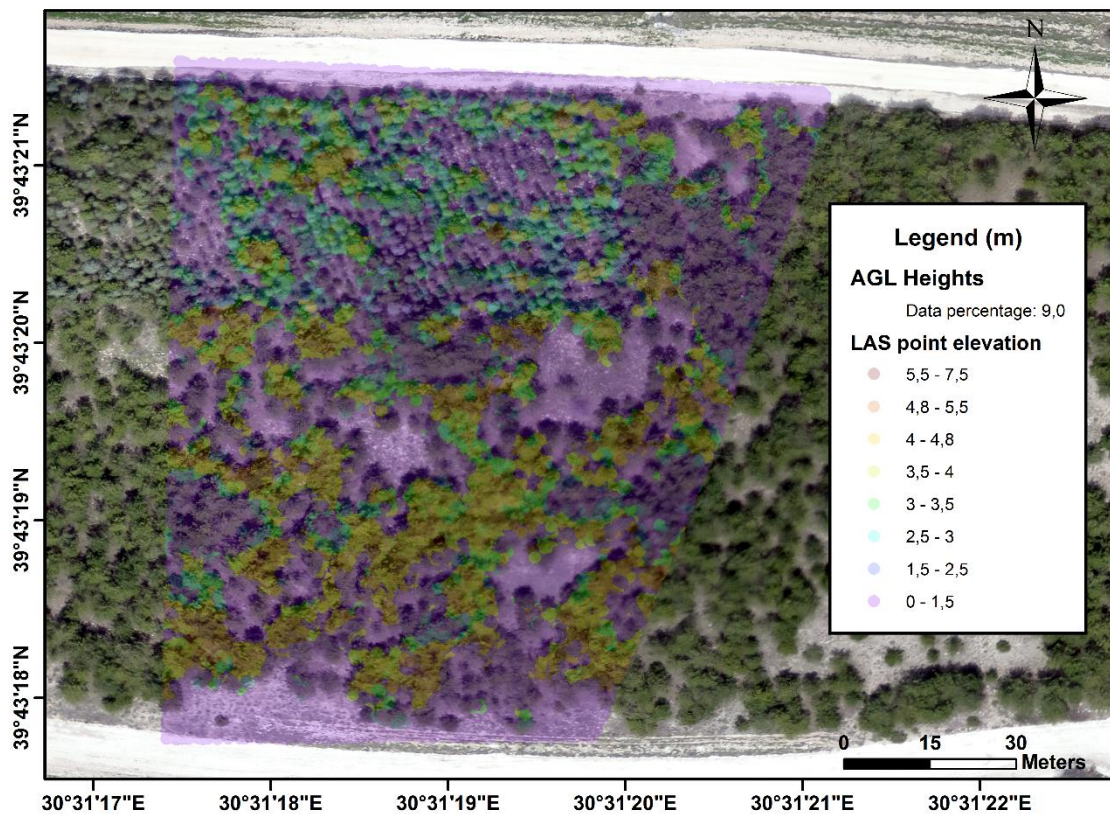


Figure 3.8. AGL height of the test area

### 3.7. Creating the Canopy Height Model

A canopy usually means the upper layer of a forest which is formed by tree crowns. CHM used in this study can be defined as above ground height model of the forest. It represents the real heights that can be easily interpreted by human eye, i.e. a tree's height can be predicted as 5.2 m, meaning the height started from the ground. The point cloud data from the AGL heights needed to be gridded into a raster in order to be filtered by local maximum filter. A step size is chosen based on the size of the trees, which would fill in a desired amount of pixels. 0.3 m step size was appropriate for the study area and a 300x400 pixel raster was created. To eliminate empty pixels within the raster, each point as classified as first returns were replaced with a circle of a predefined radius. The largest height value from the points inside pixels was used in the gridding process, therefore only one height value was embedded within pixels. Thus, the CHM was ready for validation with the ground measurements (Figure 3.9). Detailed information about how to generate flawless CHMs can be found in Khosravipour et al. [74]'s work.



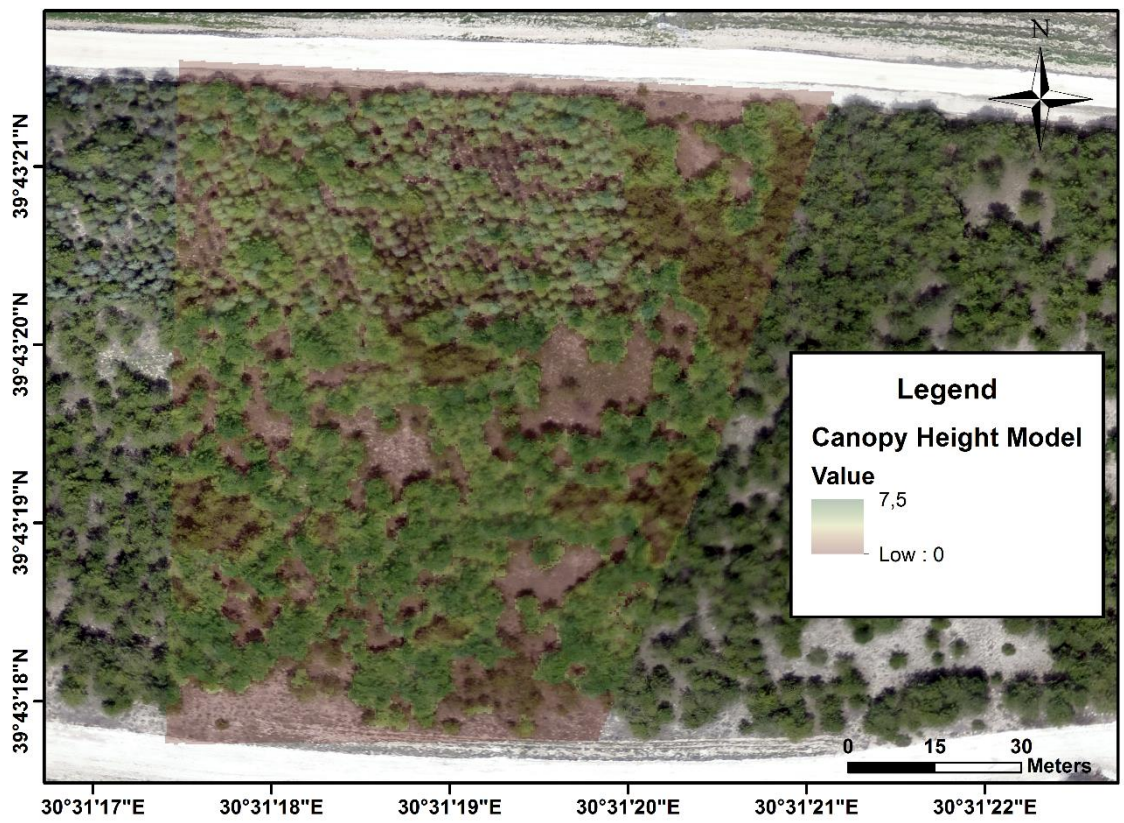


Figure 3.9. Canopy height model of the test area

## 4. RESULTS AND DISCUSSION

### 4.1. Filtering Process with Local Maximum

The CHM was based on the highest peak of the trees in the corresponding pixel. Local maximum filter is based on the window size set by the user. This filter moves the pre-defined window over the CHM and then compares the center cell's value with the surrounding pixels within a variable sized circular window in order to define the center pixel as a maximum [50, 75-77]. This algorithm uses the CHM to identify local maximums and produces a text file based result. The result can easily be imported and visualized by a Geographical Information Systems software like ArcGIS Desktop [70]. Generally, the moving window is specified as 3x3, 5x5, etc. depending on the pixel size of the CHM [50, 78, 79]. In this study, a window specified as 3x3 means that roughly in a 1m<sup>2</sup> area the algorithm would search for a maximum due to step size defined as 0.3m in the previous section. The variable sized circular window used here is based on the maximum height of the center pixel within the window size defined by the user:

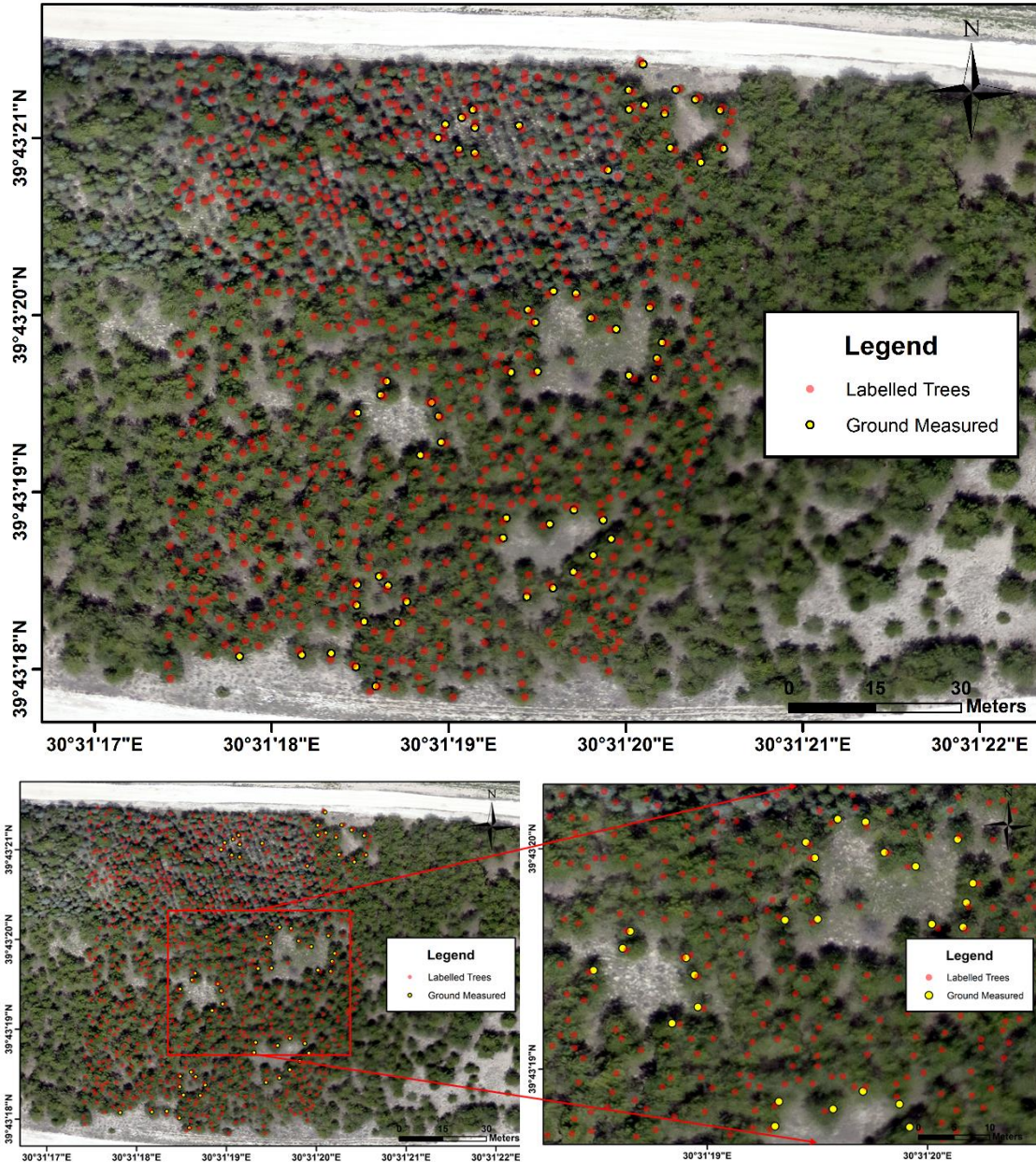
$$\text{Deciduous: Crown width (m)} = 3.09632 + 0.00895 \times ht^2 \quad (3.1)$$

$$\text{Pines: Crown width (m)} = 3.75105 - 0.17919 \times ht + 0.01241 \times ht^2 \quad (3.2)$$

$$\text{Combined: Crown width (m)} = 2.51503 + 0.00901 \times ht^2 \quad (3.3)$$

The equations are taken from [70] for deciduous, pines and combined tree types respectively. In these equations, ht represents height of the center pixel. This algorithm is calculated based on stand composition equations [70]. These equations result in tree crown radius of a tree based on its species. Height of trees are the main component of these equations to estimate a tree crown radius. Based on the ground height measurements, users should select their own window size in order to get the best results. In our study, equation 3 was selected for variable window size calculation based on the ground surveys which led the researcher believe tree crown radius in our study area differs from 2.5 m to 3 m. Radius obtained from this equation is used to draw a circle, which's center is the center pixel of the algorithm's pre-defined window as it is defined as a local maximum. Within this circle, all the pixels' values are compared to the center pixel in order to define it as the local maximum. During the process FUSION/LDV [80] software

was used. Figure 3.10 shows the resulting raster with the point features as individual trees and AGL heights.



**Figure 3.10.** Individual trees as point features obtained from CHM by using local maximum filter

#### 4.2. Validation of Estimated and Measured Tree Heights

Validation involved comparing two different methods of measuring tree height. The first method was with laser distance meter and the second was with the algorithm. In total, 53 ground-measured heights were taken. Tree heights in the test area ranged from 1.20 m to 7.10 m. A paired samples t-test were conducted due to having two population means



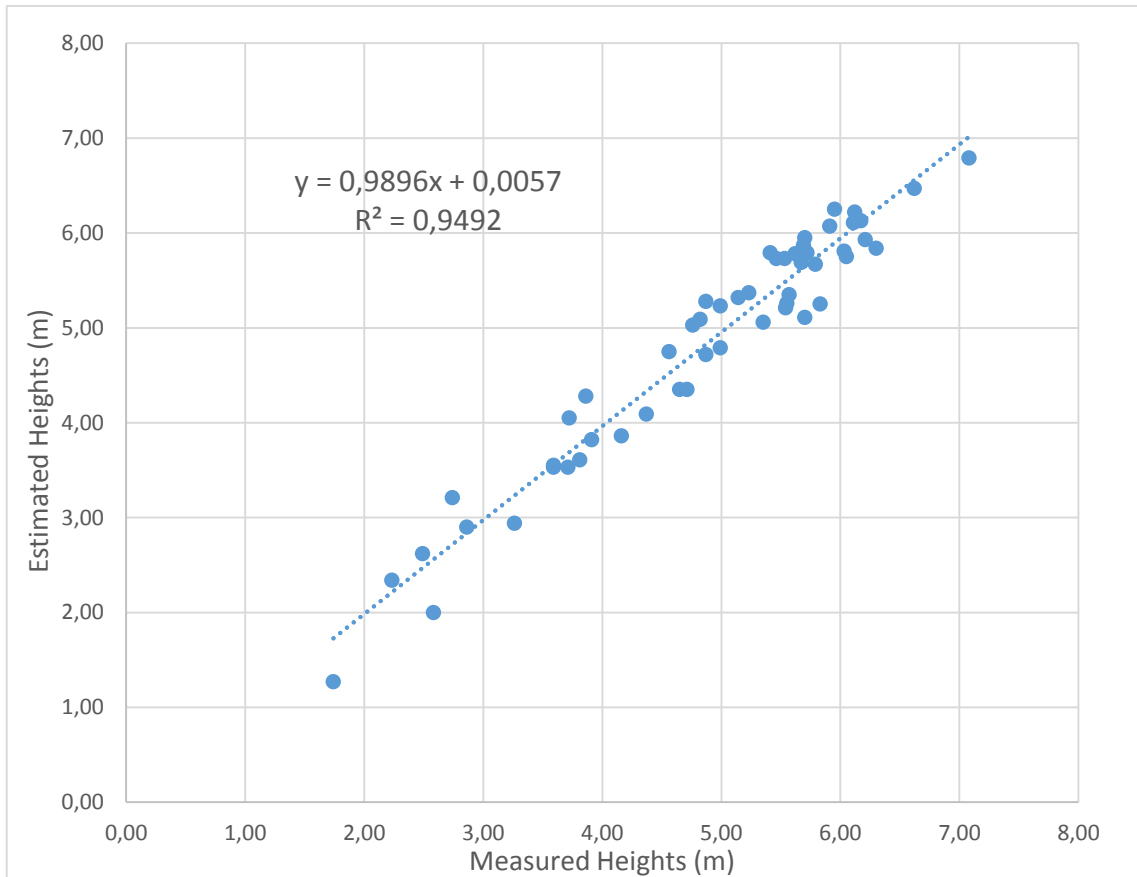
in the case of two samples that are correlated. Purpose of this statistical analysis is to determine whether the mean of differences between two paired samples differ from zero [81]. Two hypotheses are evaluated:

- $H_0$ : At %95 significance level, between ground measured and algorithm-estimated heights, there is no statistically significance ( $\mu_1-\mu_2=0$ ).
- $H_1$ : At %95 significance level, between ground measured and algorithm-estimated heights, there is statistically significance ( $\mu_1-\mu_2\neq 0$ ).

The following equation was used for paired samples t-test:

$$t = \frac{\bar{d}}{\sqrt{s^2 \div n}} \quad (3.4)$$

Where  $d$  is the mean difference between two samples,  $s^2$  is the sample variance and  $n$  is the sample size and  $t$  is a paired sample t-test with  $n-1$  degrees of freedom. “ $t$ ” value here is obtained as 1.166 which is lower than  $t$  table value defined as 2,006. Therefore we can't reject  $H_0$  null hypotheses. The correlation coefficient of the two data set was approximately 0.94 (Figure 3.11) and the root mean square error (RMSE) was 28 cm. There is no statistically significance between two data sets. In Appendix 6, a detailed table of two data set and the details of the t-test can be found.



**Figure 3.11.** Ground-measured and algorithm-estimated tree height validation results of 53 test heights (Parameters of Linear Regression and Correlation Coefficient are given in the plot).

### 4.3. Discussion

Objective of this study was to evaluate UAVs for identifying tree crowns and height for providing information to urban forest inventories. Only one previous study was identified on the quantitative validation of tree heights using UAVs with consumer-grade cameras [34]. Hence the present study and its algorithm for estimating AGL heights and positions will prove useful for forestry applications such as plant breeding, agronomy, plant quantification etc. Specifically, individual tree heights could help with growth and age classification, firewood amount prediction and probably biomass calculations. This study's main advantages are being cheaper and faster than other methods such as LiDAR, UAV-LiDAR, spaceborne LiDAR, satellite systems, and traditional photogrammetric methods. Given this study's accuracy, this approach should be useful in low-height flight sessions in order to get the best out of aerial photographs. The quality of the sensor may solve the problem of low-height flying by enabling flights at higher height, thus allowing surveys to cover more area if needed. Even so, raising the number of low- height flights



performed by small UAV platforms would still make this method more beneficial compared to other methods. Also, a necessity of GCPs are required to obtain highly accurate DEMs which later in the processing chain produces more accurate tree positions and heights.

Local tree morphologies would differently affect the performance of this methodology regardless. It is highly suggested that users should obtain their own parameters based on their ground training data. Tree crown radius is one of the key components in this methodology. Generally, in human-made forest structures, species do not differ from each other a lot. This means characteristic attributes of these trees would be similar to each other, thus making filtering process work on each tree properly. Users should gather a considerable amount of information before they start their study, tree heights for validation, tree crown radius for filtering process, tree species information etc. In our test area, detection of tree tops was easy compared to denser forests. This approach would cause problems if it is used in areas where the tree tops could not be identified because of overlapping trees, which generally occurs in natural forest areas. Clearings between trees are very helpful when it comes to interpolating the terrain beneath the forest structures. Not only clearings between trees, but also clearings within tree foliage could enable obtaining more terrain points closer to stem base. Only in very opened canopy structures this methodology can result in highly accurate results. Also, oblique photogrammetric applications would help with the resulting data's accuracy. Adjusting the interpolation process according to local parameters and obtaining more terrain points under the foliage could increase the accuracy of the data.

Ground measurements weren't homogeneously distributed over the study area. This is because, tree foliage generally didn't let the GNSS system work properly. While recording the heights with pen and paper, location of the trees could be marked on the ortho-image's paper output that has been created before ground measurements. But this method wouldn't work properly because, in a nadir perspective, locating the trees on ortho-image would be a challenging thing to do. Due to this reason, ground measurements were based on the trees which were very open from the others and could easily be identified from UAV imagery. Locations of these trees weren't the stem base location of them, but they had to be matched with the related estimated height point in order to do validation. If this method would be used in another open canopy, users should try to get as many as ground measurements as possible to validate their results.

UAVs are contributing towards flexible and cheaper sensor platforms used to obtain high quality airborne spectral and 3D-information [46]. This study proves that in human-made forest areas characterized as study's test area, tree position and tree height detection is possible through point clouds generated by image matching, thus enhancing management decisions.

## 5. CONCLUSIONS

In this study, we used a UAV and a consumer-grade camera to obtain the individual heights of trees in a forested area. Compared to other approaches, it produces accurate results, has low cost, doesn't require any trained specialists to use the UAV or the camera system and takes little time. In a 15 ha forest, we performed one flight session over 1 km<sup>2</sup> for 28 minutes and gathered 133 aerial images with 6.41 cm GSD. The aerial images were the basis for a CHM that was then filtered with a local maximum filter algorithm. The estimated tree heights from the algorithm were validated by field measurements, with a RMSE of 28 cm. Future work should focus on different types of trees and forests where the density of the forest will present the greatest challenge. With consumer-grade infrared cameras, classification of the trees should also be possible, which would provide useful data for forest inventories.

Yet this study should be performed in larger forest areas than the test area (roughly up to 1 ha, and according to a report from Republic of Turkey's General Directorate of Forestry in 2015, Turkey's forest presence is up to 22.3 million ha which covers 28.6 % of the country). This approach could prove useful when it comes to preparing inventories for very opened canopy structured forest areas and also monitoring them with a defined time interval. The highly cost effective, flexible and mobile UAV technology and with it, fully automatic photogrammetric processing chain can be taken into account for operational use.

## REFERENCES

- [1] Colomina I., Molina P. ISPRS Journal of Photogrammetry and Remote Sensing Unmanned aerial systems for photogrammetry and remote sensing : A review (2014). ISPRS J Photogramm Remote Sens [Internet]. 92:79–97. Available from: <http://dx.doi.org/10.1016/j.isprsjprs.2014.02.013>
- [2] Zarco-Tejada P.J., González-Dugo V., Berni JAJ. Fluorescence, temperature and narrow-band indices acquired from a UAV platform for water stress detection using a micro-hyperspectral imager and a thermal camera (2012). Remote Sens Environ [Internet]. 117:322–337. Available from: <http://linkinghub.elsevier.com/retrieve/pii/S0034425711003555>
- [3] Molina P., Pares M., Colomina I., Vitoria T., Silva P., Skaloud J., Kornus W., Prades R., Aguilera C. Drones to the Rescue! Unmanned aerial search missions based on thermal imaging and reliable navigation (2012). InsideGNSS 7, 36-47
- [4] Merz T., Chapman S. Autonomous unmanned helicopter system for remote sensing missions in unknown environments (2011). ISPRS, Int. Arch. Photogramm. Remote Sens. Spatial Inform. Sci. XXXVIII-1/C22, 277-282.
- [5] Rinaudo F., Chiabrando F., Lingua A., Spanò AT. Archaeological site monitoring: UAV photogrammetry can be an answer (2012). In: INTERNATIONAL ARCHIVES OF THE PHOTOGRAMMETRY, REMOTE SENSING AND SPATIAL INFORMATION SCIENCES, vol. XXXIX n. B5, pp. 583-588. ISSN 1682,1750
- [6] Manyoky M., Theiler P., Steudler D., Eisenbeiss H. Unmanned aerial vehicle in cadastral applications (2011). Int. Arch. Photogramm. Remote Sens. Spatial Inf. Sci. XXXVIII-1/C22, 57-62.
- [7] MarketsandMarkets, Unmanned Aerial Vehicles Market by Class (Small, Tactical, Strategic, Special Purpose), Subsystem (Data Link, GCS, and Software), Application (Military, Commercial and Homeland Security), Procurement by Purpose (Procurements, RDT&E, O&M), Payload & Geography - Global Forecast to 2020 (2015). MarketsandMarkets. Dallas, TX, USA.
- [8] Colomina I., Blázquez M., Molina P., Parés ME., Wis M. Towards A New Paradigm for High-Resolution Low-Cost Photogrammetry and Remote Sensing

- (2008). XXIst ISPRS Congr Tech Comm I [Internet]. XXXVII Par: 1201. Available from: [http://www.isprs.org/proceedings/XXXVII/congress/1\\_pdf/205.pdf](http://www.isprs.org/proceedings/XXXVII/congress/1_pdf/205.pdf)
- [9] Cho G., Hildebrand A., Claussen J., Cosyn P., Morris S., Pilotless aerial vehicles systems: size, scale and functions (2013). *Coordinates* 9, 8-16.
- [10] Mayr W. Unmanned aerial systems-for the rest of us (2013). In: 54<sup>th</sup> Photogrammetric Week. Institut für Photogrammetrie, Universität Stuttgart, pp. 125-134.
- [11] Petrie G. Commercial operation of lightweight UAVs for aerial imaging and mapping (2013). *GEOInformatics* 16, 28-39.
- [12] Altan M.O., Celikoyan T.M., Kemper G., Toz G. Balloon photogrammetry for cultural heritage (2004). *Int Arch Photogramm Remote Sens Spat Inf Sci.* 35.B5:964–968.
- [13] URL1: [https://en.wikipedia.org/wiki/Pigeon\\_photography#/media/File:Pigeon\\_photographers\\_and\\_aerial\\_photographs.jpg](https://en.wikipedia.org/wiki/Pigeon_photography#/media/File:Pigeon_photographers_and_aerial_photographs.jpg)
- [14] Przybilla H., Wester-Ebbinghaus W. Bildflug mit ferngelenktem Kleinflugzeug (1979). *Bildmessung and Luftbildwissen* 47, 137-142.
- [15] Wester-Ebbinghaus W. Aerial photography by radio controlled model helicopter (1980). *Photogramm. Rec.* 10, 85-92.
- [16] Ritter B. Use of Unmanned Aerial Vehicles (UAV) for Urban Tree Inventories, 2014. All theses. Paper 1890, Clemson University, South Carolina, USA.
- [17] Elias, B. Pilotless Drones: Background and Considerations for Congress Regarding Unmanned Aircraft Operations in the National Airspace System, 2012. CRS Report for Congress, Congressional Research Service 7-5700, September 10, 2012.
- [18] DIY. DIY Drones website by Chris Anderson, 2013.
- [19] URL 2: [http://arcturus-uav.com/sites/default/files/styles/gallery-full/public/product\\_slideshow/Catapult%20Launcher\\_Website.jpeg](http://arcturus-uav.com/sites/default/files/styles/gallery-full/public/product_slideshow/Catapult%20Launcher_Website.jpeg)
- [20] Eugster, H., & Nebiker, S. (2008). UAV-Based Augmented Monitoring-Real-Time Georeferencing and Integration of Video Imagery with Virtual Globes. *IAPRSSIS*, 37(B1), 1229-1235.

- [21] Eisenbess H. UAV Photogrammetry (2009). Ph.D. Thesis. Institut für Geodesie und Photogrammetrie, ETH-Zürich. Zürich, Switzerland.
- [22] Van Blyenburgh P. 2013-2014 RPAS Yearbook: Remotely Piloted Aircraft Systems: The Global Perspective 2013/2014 (2013). Technical Report. UVS International. Paris, France.
- [23] Wallace, L.; Lucieer, A.; Watson, C.; Turner, D. Development of a UAV-LiDAR System with Application to Forest Inventory (2012). *Remote Sens.*, 4, 1519–1543.
- [24] Zhou G., Yang J., Li X., Yang X. Advances of flash LIDAR development onboard UAV (2012). *ISPRS – Ann. Photogramm. Remote Sens. Spatial Inform. Sci.* XXXIX-B3, 193-198.
- [25] Remy M., de Macedo K., Moreira J. The first UAV-based P- and X-band Interferometric SAR system (2012). *IEEE*, München, Germany, pp. 5041-5044
- [26] Schulz H., The unmanned mission of avionics test helicopter – a flexible and versatile VTOL-UAS experimental system (2011). *ISPRS – Int. Arch. Photogramm. Remote Sens. Spatial Inform. Sci.* XXXVIII-1/C22, 309-314.
- [27] Essen H., Johannes W., Stanko S., Sommer R., Wahlen A., Wilcke J. High resolution W-band UAV SAR (2012). *IEEE International Geoscience and Remote Sensing Symposium (IGARSS)*, 22-27 July 2012, pp. 5033-5036.
- [28] Zhou X., Wang YC. Spatial-temporal dynamics of urban green space in response to rapid urbanization and greening policies (2011). *Landscape and Urban Planning*, 100; 268-277.
- [29] Gleason, C. J.; Im, J. Forest biomass estimation from airborne LiDAR data using machine learning approaches (2012). *Remote Sens. Environ.*, 125, 80–91.
- [30] Breidenbach, J.; Næsset, E.; Lien, V.; Gobakken, T.; Solberg, S. Prediction of species specific forest inventory attributes using a nonparametric semi-individual tree crown approach based on fused airborne laser scanning and multispectral data (2010). *Remote Sens. Environ.*, 114, 911–924.
- [31] Wallace, L.; Lucieer, A.; Watson, C. S. Evaluating tree detection and segmentation routines on very high resolution UAV LiDAR data (2014). *IEEE Trans. Geosci. Remote Sens.*, 52, 7619–7628.

- [32] Wallace, L.; Musk, R.; Lucieer, A. An assessment of the repeatability of automatic forest inventory metrics derived from UAV-borne laser scanning data (2014). *IEEE Trans. Geosci. Remote Sens.*, 52, 7160–7169.
- [33] Selkowitz, D. J.; Green, G.; Peterson, B.; Wylie, B. A multi-sensor lidar, multi-spectral and multi-angular approach for mapping canopy height in boreal forest regions (2012). *Remote Sens. Environ.* 2012, 458–471.
- [34] Zarco-Tejada, P. J.; Diaz-Varela, R.; Angileri, V.; Loudjani, P. Tree height quantification using very high resolution imagery acquired from an unmanned aerial vehicle (UAV) and automatic 3D photo-reconstruction methods (2014). *Eur J Agron* [Internet].55:89–99. Available from: <http://linkinghub.elsevier.com/retrieve/pii/S1161030114000069>
- [35] Harwin S., Lucieer A. Assessing the accuracy of georeferenced point clouds produced via multi-view stereopsis from unmanned aerial vehicle (UAV) imagery (2012). *Remote Sensing*, 4(6), 1573-1599.
- [36] Takahashi, M.; Shimada, M.; Tadono, T.; Watanabe, M. Calculation of Tree Heights Using PRISM-DSM (2012). Earth Observation Research Center, Japan Aerospace Exploration Agency., 12–15.
- [37] Gougeon, F. a; Leckie, D. G. The individual tree crown approach applied to Ikonos images of a coniferous plantation area (2006). *Photogramm. Eng. Remote Sensing*, 72, 1287–1297.
- [38] URL 3: <https://pbs.twimg.com/media/CQFFHQOWwAANwLF.png>
- [39] Sperlich, M.; Kattenborn, T.; Koch, B.; Kattenborn, G. Potential of Unmanned Aerial Vehicle Based Photogrammetric Point Clouds for Automatic Single Tree Detection (2014). *Gemeinsame Tagung 2014 der DGfK, der DGPF, der GfGI und des GIN*, 1–6.
- [40] Kattenborn, T.; Sperlich, M.; Bataua, K.; Koch, B. Automatic Single Tree Detection in Plantations using UAV-based Photogrammetric Point clouds (2014). *ISPRS - Int. Arch. Photogramm. Remote Sens. Spat. Inf. Sci.*, XL-3, 139–144.
- [41] Vauhkonen, J.; Korpela, I.; Maltamo, M.; Tokola, T. Imputation of single-tree attributes using airborne laser scanning-based height, intensity, and alpha shape metrics (2010). *Remote Sens. Environ.*, 114, 1263–1276.

- [42] Berni, J. A. J.; Zarco-Tejada, P. J.; Sepulcre-Cantó, G.; Fereres, E.; Villalobos, F. Mapping canopy conductance and CWSI in olive orchards using high resolution thermal remote sensing imagery (2009). *Remote Sens. Environ.*, 113, 2380–2388.
- [43] Küng, O.; Strecha, C.; Beyeler, A.; Zufferey, J.-C.; Floreano, D.; Fua, P.; Gervais, F. the Accuracy of Automatic Photogrammetric Techniques on Ultra-Light UAV Imagery (2011). *ISPRS - Int. Arch. Photogramm. Remote Sens. Spat. Inf. Sci.*, XXXVIII-1/, 125–130.
- [44] James, M. R.; Robson, S. Straightforward reconstruction of 3D surfaces and topography with a camera: Accuracy and geoscience application (2012). *J. Geophys. Res. Earth Surf.*, 117, 1–17.
- [45] Strecha, C.; von Hansen, W.; Van Gool, L.; Fua, P.; Thoennessen, U. On benchmarking camera calibration and multi-view stereo for high resolution imagery (2008). *2008 IEEE Conf. Comput. Vis. Pattern Recognit.*, 1–8.
- [46] Vallet, J.; Panissod, F.; Strecha, C.; Tracol, M. Photogrammetric Performance of an Ultra Light Weight Swinglet “Uav.” (2012). *ISPRS - Int. Arch. Photogramm. Remote Sens. Spat. Inf. Sci.*, XXXVIII-1/, 253–258.
- [47] Fritz, a.; Kattenborn, T.; Koch, B. Uav-Based Photogrammetric Point Clouds – Tree Stem Mapping in Open Stands in Comparison To Terrestrial Laser Scanner Point Clouds (2013). *ISPRS - Int. Arch. Photogramm. Remote Sens. Spat. Inf. Sci.*, XL-1/W2, 141–146.
- [48] Remondino, F.; Barazzetti, L.; Nex, F.; Scaioni, M.; Sarazzi, D. Uav Photogrammetry for Mapping and 3D Modeling – Current Status and Future Perspectives (2011). *Int. Arch. Photogramm.*, XXXVIII, 14–16.
- [49] Wallerman, J.; Bohlin, J.; Fransson, J. E. S. Forest height estimation using semi-individual tree detection in multi-spectral 3D aerial DMC data (2012). *Geosci. Remote Sens. Symp. (IGARSS), 2012 IEEE Int.*, 6372–6375.
- [50] Waser, L. T.; Baltsavias, E.; Ecker, K.; Eisenbeiss, H.; Ginzler, C.; Küchler, M.; Thee, P.; Zhang, L. High-resolution digital surface models (DSMs) for modelling fractional shrub/tree cover in a mire environment (2008). *Int. J. Remote Sens.*, 29, 1261–1276.



- [51] Popescu, S. C.; Wynne, R. H.; Nelson, R. F. Estimating plot-level tree heights with lidar: Local filtering with a canopy-height based variable window size (2003). *Comput. Electron. Agric.*, 37, 71–95.
- [52] Packalén P., Maltamo M. The k-MSN method for the prediction of species-specific stand attributes using airborne laser scanning and aerial photographs (2007). *Remote Sens Environ* [Internet]. 109:328–341. Available from: <http://www.sciencedirect.com/science/article/pii/S0034425707000387>
- [53] Monnet JM., Mermin E., Chanussot J., Berger F. Tree top detection using local maxima filtering: a parameter sensitivity analysis (2010). 10th International Conference on LiDAR Applications for Assessing Forest Ecosystems (Silvilaser 2010), Sep 2010, Freiburg, Germany. 9 p. <hal-00523245>
- [54] Vauhkonen J., Ene L., Gupta S., Heinzl J., Holmgren J., Pitkanen J., Solberg S., Wang Y., Weinacker H., Hauglin KM., et al.. Comparative testing of single-tree detection algorithms under different types of forest (2012). *Forestry* [Internet]. 85:2740. <http://forestry.oxfordjournals.org/cgi/doi/10.1093/forestry/cpr051>
- [55] Waser LT., Ginzler C., Kuechler M., Baltsavias E., Hurni L. Semi-automatic classification of tree species in different forest ecosystems by spectral and geometric variables derived from Airborne Digital Sensor (ADS40) and RC30 data (2011). *Remote Sens Environ* [Internet]. 115:76–85. Available from: <http://linkinghub.elsevier.com/retrieve/pii/S0034425710002464>
- [56] Zarco-Tejada PJ., Guillén-Climent ML., Hernández-Clemente R., Catalina A., González MR., Martín P. Estimating leaf carotenoid content in vineyards using high resolution hyperspectral imagery acquired from an unmanned aerial vehicle (UAV) (2013). *Agric For Meteorol* [Internet]. 171-172:281–294. Available from: <http://dx.doi.org/10.1016/j.agrformet.2012.12.013>
- [57] Chen Q., Baldocchi D., Gong P., Kelly M. Isolating Individual Trees in a Savanna Woodland Using Small Footprint Lidar Data (2006). *Photogramm. Eng. Remote Sens* [Internet]. 72:923–932. Available from: <http://essential.metapress.com/openurl.asp?genre=article&>
- [58] Kaartinen H., Hyypä J. EuroSDR/ISPRS Commission II project: “Tree Extraction”—final report (2008). Official publication no. 53. EuroSDR, Frankfurt am Main, Germany, 60 p.

- [59] Gupta S., Koch B., Weinacker H. Tree species detection using full waveform lidar data in a complex forest (2010). In Technical Commission VII Symposium—100 Years of ISPRS Vienna, Austria, July 5–7, 2010. W. Wagner and B. Székely (eds). Vienna University of Technology, Vienna, Austria, pp. 249–254.
- [60] Wang Y., Weinacker H., Koch B., Sterenczak K. Lidar point cloud based fully automatic 3D single tree modelling in forest and evaluations of the procedure (2008). *Int. Archives Photo- grammetry Remote Sens Spatial Inform. Sci.* XXXVII, 45–51.
- [61] Ene L., Næsset E., Gobakken T. Single tree detection in heterogeneous boreal forests using airborne laser scanning and area based stem number estimates (2011). *Int. J. Remote Sens.*
- [62] Ben-Arie JR., Hay GJ., Powers RP., Castilla G., St-Onge B. Development of a pit filling algorithm for LiDAR canopy height models (2009). *Comput. Geosci.* 35, 1940–1949.
- [63] Solberg S., Næsset E., Bollandsås OM. Single tree segmentation using airborne laser scanner data in a hetero-geneous spruce forest (2006). *Photogramm. Eng. Remote Sens.* 72, 1369–1378.
- [64] Pollock RJ. The automatic recognition of individual trees in aerial images of forests based on a synthetic tree crown image model (1996). Ph.D. Thesis. University of British Columbia, Vancouver, Canada. 172 pp.
- [65] Holmgren J., Wallerman J. Estimation of tree size distribution by combining vertical and horizontal distribution of LIDAR measurements with extraction of individual trees (2006). In Workshop on 3D Remote Sensing in Forestry, 14–15 February 2006. T. Koukal and W. Schneider (eds). University of Natural Resources and Applied Life Science, Vienna, Austria, pp. 168–173.
- [66] Holmgren J., Barth A., Larsson H., Olsson H. Prediction of stem attributes by combining airborne laser scanning and measurements from harvesting machinery (2010). *SilviLaser 2010, the 10th International Conference on LiDAR Applications for Assessing Forest Ecosystems*, 14–17 September 2010, Freiburg, Germany, Proceedings USB disc, 10 pp.
- [67] Pitkänen J., Maltamo M., Hyyppä J., Yu X. Adaptive methods for individual tree detection on airborne laser based canopy height model (2004). In Proceedings of

- ISPRS Working Group VIII/2: “Laser-scanners for forest and landscape assessment”. M. Theis, B. Koch, H. Spiecker and H. Weinacker (eds). University of Freiburg, Germany, pp. 187–191.
- [68] Hunt, E. R.; Cavigelli, M.; Daughtry, C. S. T.; McMurtrey, J. E.; Walthall, C. L. Evaluation of digital photography from model aircraft for remote sensing of crop biomass and nitrogen status (2005). *Precis. Agric.*, 6, 359–378.
- [69] Hongoh, D.; Kajiwara, K.; Honda, Y. Developing Ground Truth Measurement System using RC Helicopter and BRDF Model in Forest Area 3 (2001). *MODELS OF BI-DIRECTIONAL REFLECTANCE.*, 5–9.
- [70] ESRI 2011. ArcGIS Desktop: Release 10. Redlands, CA: Environmental Systems Research Institute. <http://resources.arcgis.com/en/home/>
- [71] Pix4D – Drone Mapping Software 2014. Swiss Federal Institute of Technology Lausanne, Route Cantonale, Switzerland. <https://pix4d.com/>
- [72] Schönberger, J.L., Fraundorfer, F., Frahm, J.M. Structure-from-motion for MAV image sequence analysis with photogrammetric applications (2014). *Int Arch Photogramm Remote Sens Spat Inf Sci - ISPRS Arch.* 40:305–312.
- [73] Rapidlosso, 2014. Creator of LASTools for LiDAR. <http://rapidlosso.com>
- [74] Khosravipour, A., Skidmore A.K., Isenburg, M., Wang, T.J., Hussin Y.A. Generating pit-free Canopy Height Models from Airborne LiDAR (2014). *PE&RS: Photogrammetric Engineering and Remote Sensing* 80, 863-872.
- [75] Kini, A. U.; Popescu, S. C. TreeVaW: a versatile tool for analyzing forest canopy LIDAR data: A preview with an eye towards future (2004). In CD-ROM Proceedings, ASPRS 2004 Fall Conference, Kansas City, Missouri.
- [76] Popescu, Sorin C., and Randolph H. Wynne. Seeing the trees in the forest (2004). *Photogrammetric Engineering & Remote Sensing* 70.5., 589-604.
- [77] McGaughey, R.J. FUSION/LDV: Software for LIDAR Data Analysis and Visualization (2014). User-Manual., page: 25-27
- [78] Niemann, K. O., Adams, S., Hay, G. Automated Tree Crown Identification Using Digital Orthophoto Mosaics (1998). *Proceedings of the International Forum on Automated Interpretation of High Spatial Resolution Digital Imagery for Forestry*, pp. 105-112

- [79] Pinz, A. Tree Isolation and Species Classification (1998). Proceedings of the International Forum on Automated Interpretation of High Spatial Resolution Digital Imagery for Forestry, pp. 127-139
- [80] FUSION/LDV: Software for LiDAR Data Analysis and Visualization (2014). FUSION Version 3.42. United States Department of Agriculture, Forest Service, Pacific Northwest Station.  
<http://forsys.cfr.washington.edu/fusion/fusionlatest.html>
- [81] Daniel, W. W., Terrell J. C. Business Statistics For Management And Economics, Seventh Edition (1995). Houghton Mifflin Company, Boston, Toronto.


## APPENDIX



### Appendix 1 – Quality report of the photogrammetric process

# Quality Report



Generated with version 3.2.82

 **Important:** Click on the different icons for:

-  Help to analyze the results in the Quality Report
-  Additional information about the feature

 For additional tips to analyze the Quality Report, click [here](#).

#### Summary



Project	2015_04_25_anil_6cm_kent
Processed	2015-Apr-25 17:30:53
Camera Model Name	CanonIXUS127HS_4.3_4608x3456 (RGB)
Average Ground Sampling Distance (GSD)	6.41 cm / 2.52 in
Area Covered	0.7061 km <sup>2</sup> / 70.61 ha / 0.2728 sq. mi. / 174.571 acres
Image Coordinate System	WGS84
Ground Control Point (GCP) Coordinate System	WGS 84 / UTMzone 36N
Output Coordinate System	WGS 84 / UTMzone 36N
Processing Type	full aerial nadir
Feature Extraction Image Scale	1
Camera Model Parameter Optimization	optimize externals and all internals
Time for Initial Processing (without report)	27m:53s

## Quality Check



🔍 Images	median of 60991 keypoints per image	✓
🔍 Dataset	133 out of 133 images calibrated (100%), all images enabled	✓
🔍 Camera Optimization	0.06% relative difference between initial and final focal length	✓
🔍 Matching	median of 11385.5 matches per calibrated image	✓
🔍 Georeferencing	6 GCPs (6 3D), mean error = 0.041 m	✓

## 🔍 Preview

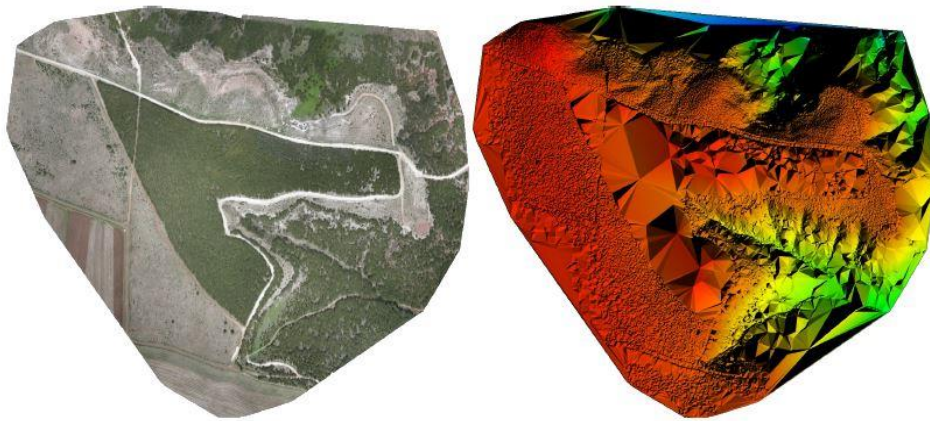


Figure 1: Orthomosaic and the corresponding sparse Digital Surface Model (DSM) before densification.

## Calibration Details



Number of Calibrated Images	133 out of 133
Number of Geolocated Images	133 out of 133

## 🔍 Initial Image Positions

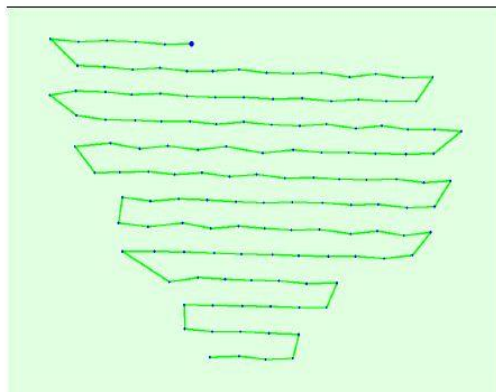


Figure 2: Top view of the initial image position. The green line follows the position of the images in time starting from the large blue dot.

### Computed Image/GCPs/Manual Tie Points Positions

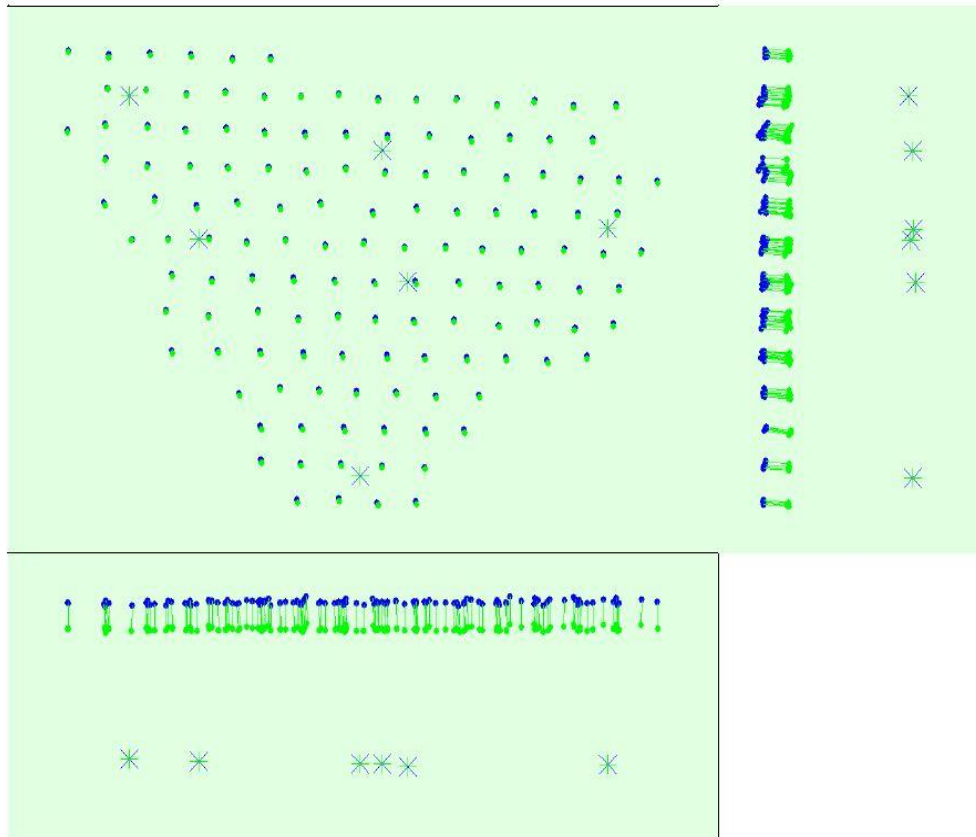


Figure 3: Offset between initial (blue dots) and computed (green dots) image positions as well as the offset between the GCPs initial positions (blue crosses) and their computed positions (green crosses) in the top-view (XY plane), front-view (XZ plane), and side-view (YZ plane).

### Overlap

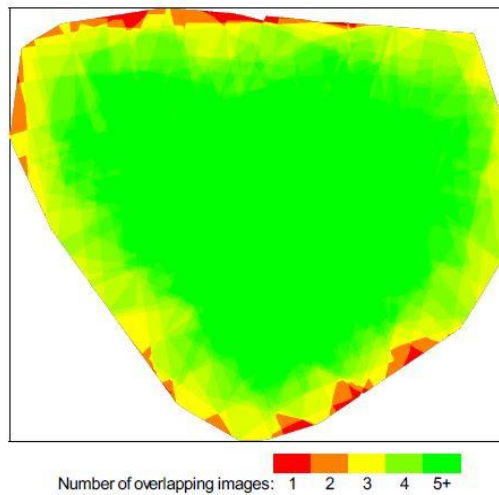


Figure 4: Number of overlapping images computed for each pixel of the orthomosaic. Red and yellow areas indicate low overlap for which poor results may be generated. Green areas indicate an overlap of over 5 images for every pixel. Good quality results will be generated as long as the number of keypoint matches is also sufficient for these areas (see Figure 5 for keypoint matches).



## Bundle Block Adjustment Details



Number of 2D Keypoint Observations for Bundle Block Adjustment	1752447
Number of 3D Points for Bundle Block Adjustment	587230
Mean Reprojection Error [pixels]	0.300398

### Internal Camera Parameters

CanonIXUS127HS\_4.3\_4608x3456 (RGB). Sensor Dimensions: 6.17 [mm] x 4.63 [mm]



EXIF ID: CanonIXUS127HS\_4.3\_4608x3456

	Focal Length	Principal Point x	Principal Point y	R1	R2	R3	T1	T2
Initial Values	3270.924 [pixel] 4.380 [mm]	2303.999 [pixel] 3.085 [mm]	1728.000 [pixel] 2.314 [mm]	-0.049	0.059	-0.036	0.000	-0.003
Optimized Values	3273.155 [pixel] 4.383 [mm]	2427.427 [pixel] 3.250 [mm]	1817.891 [pixel] 2.434 [mm]	-0.041	0.034	-0.008	0.006	0.009

### 2D Keypoints Table



	Number of 2D Keypoints per Image	Number of Matched 2D Keypoints per Image
Median	60991	11386
Mn	16675	887
Max	74928	27202
Mean	57479	13176

### 3D Points from 2D Keypoint Matches



	Number of 3D Points Observed
In 2 Images	358507
In 3 Images	105017
In 4 Images	47372
In 5 Images	25949
In 6 Images	16301



In 7 Images	10914
In 8 Images	7612
In 9 Images	5318
In 10 Images	3626
In 11 Images	2587
In 12 Images	1709
In 13 Images	937
In 14 Images	627
In 15 Images	368
In 16 Images	211
In 17 Images	92
In 18 Images	57
In 19 Images	14
In 20 Images	4
In 21 Images	5
In 22 Images	3

### 3D Points from 2D Keypoint Matches

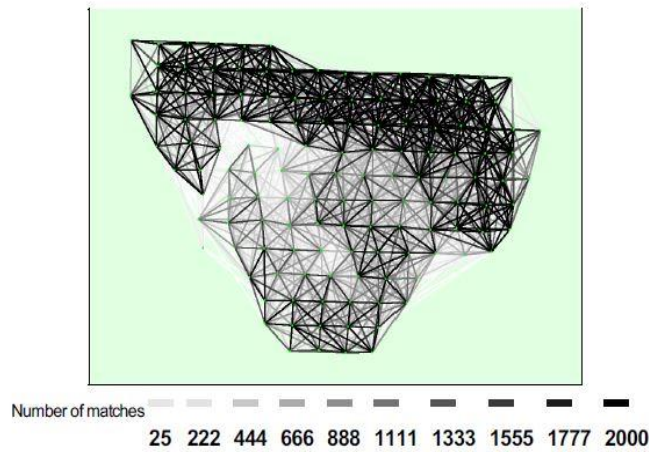


Figure 5: Top view of the image computed positions with a link between matching images. The darkness of the links indicates the number of matched 2D keypoints between the images. Bright links indicate weak links and require manual tie points or more images.

## Geolocation Details

### Ground Control Points

GCP Name	Accuracy XY/Z [m]	Error X [m]	Error Y [m]	Error Z [m]	Projection Error [pixel]	Verified/Marked
k1 (3D)	0.020/ 0.020	-0.007	0.020	-0.067	0.669	5 / 5
k2 (3D)	0.020/ 0.020	-0.029	0.004	0.133	0.468	5 / 5
k3 (3D)	0.020/ 0.020	-0.016	-0.042	-0.124	0.510	5 / 5
k4 (3D)	0.020/ 0.020	0.003	-0.016	0.032	0.741	5 / 5
k5 (3D)	0.020/ 0.020	0.026	-0.004	0.002	0.757	4 / 4
k6 (3D)	0.020/ 0.020	0.025	0.028	0.027	0.731	5 / 5
<b>Mean</b>		0.000131	-0.001746	0.000630		
<b>Sigma</b>		0.020261	0.023253	0.081073		
<b>RMS Error</b>		0.020262	0.023318	0.081076		

Localisation accuracy per GCP and mean errors in the three coordinate directions. The last column counts the number of images where the GCP has been automatically verified vs. manually marked.

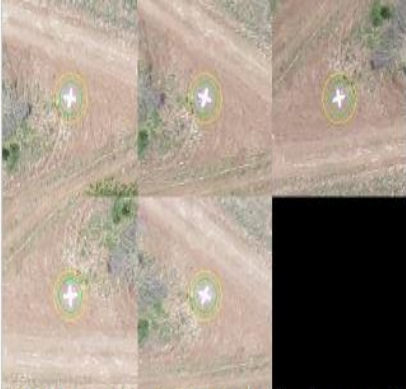

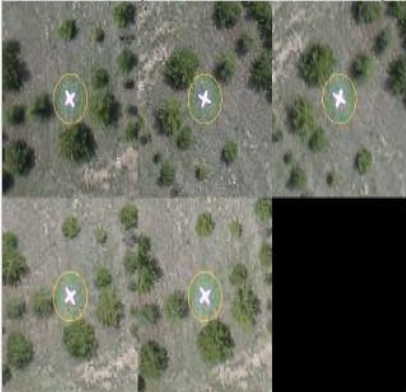
### Absolute Geolocation Variance

Mn Error [m]	MaxError [m]	Geolocation Error X[%]	Geolocation Error Y[%]	Geolocation Error Z[%]
-	-9.41	0.00	0.00	0.00
-9.41	-7.53	0.00	0.00	0.00
-7.53	-5.64	0.00	0.00	0.00
-5.64	-3.76	0.00	0.00	0.00
-3.76	-1.88	3.01	0.00	0.00
-1.88	0.00	75.94	0.00	0.00
0.00	1.88	21.05	0.75	0.00
1.88	3.76	0.00	55.64	0.00
3.76	5.64	0.00	43.61	0.00
5.64	7.53	0.00	0.00	0.00
7.53	9.41	0.00	0.00	0.00
9.41	-	0.00	0.00	100.00
<b>Mean</b>		-0.619786	3.637876	39.925570
<b>Sigma</b>		0.693443	0.828137	1.111058
<b>RMS Error</b>		0.930053	3.730945	39.941027


Min Error and Max Error represent geolocation error intervals between -1.5 and 1.5 times the maximum accuracy of all the images. Columns X, Y, Z show the percentage of images with geolocation errors within the predefined error intervals. The geolocation error is the difference between the initial and computed image positions. Note that the image geolocation errors do not correspond to the accuracy of the observed 3D points.

**Georeference Verification**



GCP Name: k1 (287092.18,4399841.94,999.28)	
	IMG_6675.JPG IMG_6676.JPG IMG_6680.JPG IMG_6681.JPG IMG_6702.JPG
GCP k1 was not marked in the following images (only up to 6 images shown). If the circle is too far away from the initial GCP position, also measure the GCP in these images to improve the accuracy.	
	IMG_6617.JPG IMG_6645.JPG IMG_6647.JPG IMG_6652.JPG IMG_6653.JPG IMG_6677.JPG
GCP Name: k2 (286978.70,4400056.57,1002.73)	
	IMG_6621.JPG IMG_6623.JPG IMG_6624.JPG IMG_6648.JPG IMG_6649.JPG

GCP k2 was not marked in the following images (only up to 6 images shown). If the circle is too far away from the initial GCP position, also measure the GCP in these images to improve the accuracy.




IMG\_6618.JPG  
 IMG\_6620.JPG  
 IMG\_6646.JPG  
 IMG\_6647.JPG  
 IMG\_6651.JPG

GCP Name: k3 (287391.70,4399974.83,995.41)



IMG\_6631.JPG  
 IMG\_6642.JPG  
 IMG\_6643.JPG  
 IMG\_6657.JPG  
 IMG\_6658.JPG

GCP k3 was not marked in the following images (only up to 6 images shown). If the circle is too far away from the initial GCP position, also measure the GCP in these images to improve the accuracy.



IMG\_6627.JPG  
 IMG\_6628.JPG  
 IMG\_6629.JPG  
 IMG\_6630.JPG  
 IMG\_6640.JPG  
 IMG\_6641.JPG



GCP Name: k4 (287759.66,4399857.19,994.21)

	<p>IMG_6663.JPG          IMG_6664.JPG          IMG_6667.JPG          IMG_6690.JPG          IMG_6691.JPG</p>
<p>GCP k4 was not marked in the following images (only up to 6 images shown). If the circle is too far away from the initial GCP position, also measure the GCP in these images to improve the accuracy.</p>	
	<p>IMG_6635.JPG          IMG_6637.JPG          IMG_6662.JPG          IMG_6665.JPG          IMG_6666.JPG          IMG_6689.JPG</p>

GCP Name: k5 (287433.12,4399777.89,990.84)

	<p>IMG_6686.JPG          IMG_6698.JPG          IMG_6699.JPG          IMG_6710.JPG</p>
<p>GCP k5 was not marked in the following images (only up to 6 images shown). If the circle is too far away from the initial GCP position, also measure the GCP in these images to improve the accuracy.</p>	
	<p>IMG_6642.JPG          IMG_6655.JPG          IMG_6658.JPG          IMG_6659.JPG          IMG_6669.JPG          IMG_6670.JPG</p>

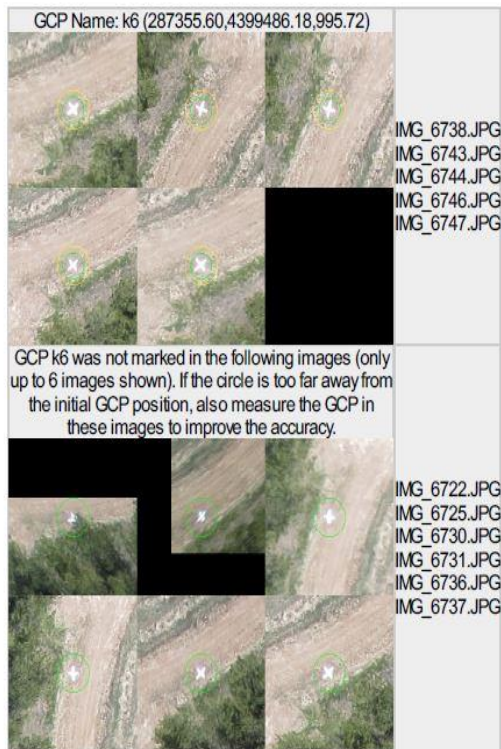


Figure 7: Images in which GCPs have been marked (yellow circle) and in which their computed 3D points have been projected (green circle). A green circle outside of the yellow circle indicates either an accuracy issue or a GCP issue.

## Point Cloud Densification details

### Summary

Processing Type	aerial nadir
Image Scale	multiscale, 1 (original image size, slow)
Point Density	optimal
Minimum Number of Matches	3
Use Densification Area	yes
Use Annotations	yes
Use Noise Filtering	yes, radius = 10 GSD
Use Surface Smoothing	yes, sharp, radius = 10 GSD
Time for Densification and Filtering (without report)	03h:44m:29s

### Results

Number of Processed Clusters	2
Number of 3D Densified Points	62919961
Number of 3D Filtered Points	35003614
Average Density (per m <sup>3</sup> )	40.92

## Appendix 2 - Technical Specifications of Canon IXUS 127 HS

<b>Specifications</b>	
Camera Effective Pixels	Approx. 16.1 million pixels
Lens Focal Length	5x zoom: 4.3 (W) – 21.5 (T) mm (35mm film equivalent: 24 (W) – 120 (T) mm)
LCD Monitor	7.5 cm (3.0 in.) color TFT LCD Effective Pixels: Approx. 461,000 dots
File Formats	Design rule for Camera File system, DPOF (version 1.1) compliant
Data Types	Still Images: Exif 2.3 (JPEG) Movies: MOV (H.264 video data, Linear PCM (2 channel monaural) audio data)
Interfaces	Hi-speed USB HDMI output Analog audio output (monaural) Analog video output (NTSC/PAL)
Power	Battery Pack NB-11L AC Adapter Kit ACK-DC90
Dimensions (Based on CIPA Guidelines)	93.2 x 57.0 x 20.0 mm (3.67 x 2.24 x 0.79 in.)
Weight (Based on CIPA Guidelines)	Approx. 135 g (approx. 4.76 oz.; including batteries and memory card) Approx. 120 g (approx. 4.23 oz.; camera body only)



### Number of Shots/Recording Time, Playback Time









<b>Number of Shots</b>	Approx. 170
<b>Movie Recording Time<sup>*1</sup></b>	Approx. 30 minutes
<b>Continuous Shooting<sup>*2</sup></b>	Approx. 1 hour
<b>Playback Time</b>	Approx. 3 hours

\*1 Time under default camera settings, when normal operations are performed, such as shooting, pausing, turning the camera on and off, and zooming.

\*2 Time available when shooting the maximum movie length (until recording stops automatically) repeatedly.

- The number of shots that can be taken is based on measurement guidelines of the Camera & Imaging Products Association (CIPA).
- Under some shooting conditions, the number of shots and recording time may be less than mentioned above.
- Number of shots/recording time with fully charged batteries.

### Number of 4:3 Shots per Memory Card

Resolution (Pixels)	Compression Ratio	No. Shots per Memory Card (Approx.)	
		8 GB	32 GB
<b>L</b> (Large) 16M/4608x3456		1131	4567
		1903	7684
<b>M1</b> (Medium 1) 8M/3264x2448		2252	9094
		3721	15020
<b>M2</b> (Medium 2) 2M/1600x1200		7442	30040
		12927	52176
<b>S</b> (Small) 0.3M/640x480		27291	110150
		40937	165225

- These values are measured according to Canon standards and may change depending on the subject, memory card and camera settings.

- Table values are based on images with a 4:3 aspect ratio. Changing the aspect ratio (see p. 71) will enable more shots, because less data is used per image than for 4:3 images. However, with **M2**, 16:9 images have a resolution of 1920 x 1080 pixels, which requires more data than for 4:3 images.



## Recording Time per Memory Card

Image Quality	Recording Time per Memory Card	
	8 GB	32 GB
	29 min. 39 sec.	1 hr. 59 min. 43 sec.
	42 min. 11 sec.* <sup>1</sup>	2 hr. 50 min. 19 sec.* <sup>2</sup>
	1 hr. 28 min. 59 sec.	5 hr. 59 min. 10 sec.

\*<sup>1</sup> Approx. 27 min. 39 sec. for iFrame movies (see p. 104).

\*<sup>2</sup> Approx. 1 hr. 51 min. 37 sec. for iFrame movies (see p. 104).

- These values are measured according to Canon standards and may change depending on the subject, memory card and camera settings.
- Recording will automatically stop when the file size of an individual clip being recorded reaches 4 GB, or when the recording time reaches approximately 10 minutes (for or movies) or approximately 1 hour (for movies).
- On some memory cards, recording may stop before the maximum clip length has been reached. Speed Class 6 or higher memory cards are recommended.

## Flash Range

Maximum wide angle ()	50 cm – 3.5 m (1.6 – 11 ft.)
Maximum telephoto ()	90 cm – 2.0 m (3.0 – 6.6 ft.)

## Shooting Range

Shooting Mode	Focusing Range	Maximum Wide Angle ()	Maximum Telephoto ()
	–	3 cm (1.2 in.) – infinity	90 cm (3.0 ft.) – infinity
Other modes		5 cm (2.0 in.) – infinity	90 cm (3.0 ft.) – infinity
	*	3 – 50 cm (1.2 in. – 1.6 ft.)	–
	*	3 m (9.8 ft.) – infinity	3 m (9.8 ft.) – infinity

\* Not available in some shooting modes.

## Continuous Shooting Speed

Shooting Mode	Speed
	Approx. 5.8 shots/sec.
<b>P</b>	Approx. 2.0 shots/sec.

### ▼ Shutter Speed

<b>AUTO</b> mode, automatically set range	1 – 1/2000 sec.
Range in all shooting modes	15 – 1/2000 sec.

### ▼ Aperture

f/number	f/2.7 / f/8.0 (W), f/5.9 / f/17 (T)
----------	-------------------------------------

### ▼ Battery Pack NB-11L

Type	Rechargeable lithium-ion battery
Rated Voltage	3.6 V DC
Rated Capacity	680 mAh
Charging Cycles	Approx. 300 times
Operating Temperature	0 – 40 °C (32 – 104 °F)
Dimensions	34.6 x 40.2 x 5.2 mm (1.36 x 1.58 x 0.20 in.)
Weight	Approx. 13 g (approx. 0.46 oz.)

### ▼ Battery Charger CB-2LD/CB-2LDE

Rated Input	100 V – 240 V AC (50/60 Hz)
Rated Output	4.2 V DC, 0.41 A
Charging Time	Approx. 2 hours (when using NB-11L)
Charge Indicator	Charging: orange / Fully charged: green (two-indicator system)
Operating Temperature	5 – 40 °C (41 – 104 °F)
Dimensions	85.0 x 57.6 x 24.3 mm (3.35 x 2.27 x 0.96 in.)
Weight	Approx. 59 g (approx. 2.08 oz.) (CB-2LD) Approx. 56 g (approx. 1.98 oz.) (CB-2LDE, excluding power cord)

- All data is based on tests by Canon.
- Camera specifications or appearance are subject to change without notice.

## Appendix 3 – Technical Specifications of Leica DISTO D810 Laser Meter

### Technical Data

EN

Distance measurement	
Typical Measuring Tolerance*	$\pm 1.0 \text{ mm} / \sim 1/16''$ ***
Maximum Measuring Tolerance**	$\pm 2.0 \text{ mm} / 0.08 \text{ in}$ ***
Typical Range*	250 m / 820 ft
Range at unfavourable condition ****	120 m / 394 ft
Smallest unit displayed	0.1 mm / 1/32 in
Power Range Technology™	yes
Ø laser point at distances	6 / 30 / 60 mm (10 / 50 / 100 m)

Tilt measurement	
Measuring tolerance to laser beam*****	$-0.1^\circ / +0.2^\circ$
Measuring tolerance to housing*****	$\pm 0.1^\circ$
Range	360°

General	
Laser class	2
Laser type	635 nm, < 1 mW
Protection class	IP54 (dust- and splash water protected)
Autom. laser switch off	after 90 s
Autom. power switch-off	after 180 s
Bluetooth® Smart	Bluetooth v4.0
Range of Bluetooth®	< 10 m
Dimension (H x D x W)	61 x 31 x 164 mm 2.4 x 1.2 x 6.5 in
Weight	238 g / 8.4 oz
Temperature range:	
- Storage	-25 to 60 °C -13 to 140 °F
- Operation	-10 to 50 °C 14 to 122 °F
- Charging	-10 to 40 °C 14 to 104 °F

Photos / Screenshots	
Resolution for photos	800 x 600 dpi
Resolution for screenshots	240 x 400 dpi
File format	JPG
Download of gallery	USB

Battery (Li-Ion)	
Rated voltage	3.7 V
Capacity	2.6 Ah
Measurements per battery charge	Approx. 4000
Charging time	Approx. 4 h
Output voltage	5.0 V
Charging current	1 A

\* applies for 100 % target reflectivity (white painted wall), low background illumination, 25 °C

\*\* applies for 10 to 100 % target reflectivity, high background illumination, - 10 °C to + 50 °C

\*\*\* Tolerances apply from 0.05 m to 10 m with a confidence level of 95%. The maximum tolerance may deteriorate to 0.1 mm/m between 10 m to 30 m, to 0.20 mm/m between 30 m to 100 m and to 0.30 mm/m for distances above 100 m

\*\*\*\* applies for 100 % target reflectivity, background illumination of approximately 30'000 lux

\*\*\*\*\* after user calibration. Additional angle related deviation of +/- 0.01° per degree up to +/-45° in each quadrant.

Applies at room temperature. For the whole operating temperature range the maximum deviation increases by +/-0.1°.

**i** At a recommended storage temperature of -20°C to +30°C (-4°F to +86°F), batteries containing a 50% to 100% charge can be stored up to 1 year. After this storage period the batteries must be recharged.

**i** For accurate indirect results, the use of a tripod is recommended. For accurate tilt measurements a transverse tilt should be avoided.



## Appendix 4 - Technical Specifications of eBee UAV of senseFly

### HARDWARE

Wingspan	96 cm (37.8 in)
Weight (inc. supplied camera & battery)	Approx. 0.69 kg (1.52 lb)
Motor	Low-noise, brushless, electric
Radio link range	Up to 3 km (1.86 miles)
Detachable wings	Yes
Camera (supplied)*	WX RGB (18.2 MP)
Cameras (optional)	S110 NIR/RE/RGB, Sequoia, thermoMAP

### SOFTWARE

Flight planning & control software (supplied)	eMotion
Image processing software (optional)	Pix4Dmapper Pro

### OPERATION

Automatic 3D flight planning	Yes
Cruise speed	40-90 km/h (11-25 m/s or 25-56 mph)
Wind resistance	Up to 45 km/h (12 m/s or 28 mph)
Maximum flight time	50 minutes
Maximum coverage (single flight)	12 km <sup>2</sup> (4.6 mi <sup>2</sup> )**
Automatic landing	Linear landing with ~ 5 m (16.4 ft) accuracy
Multi-drone operation	Yes
Ground control points (GCPs)	Optional
Oblique imagery	0 to -50°

### RESULTS

Ground sampling distance (GSD)	Down to 1.5 cm (0.6 in) / pixel***
Absolute horizontal/vertical accuracy (w/GCPs)	Down to 3 cm (1.2 in) / 5 cm (2 in)
Absolute horizontal/vertical accuracy (no GCPs)	1-5 m (3.3-16.4 ft)

\*Optional in Turkey.

\*\* Based on the following test conditions: target ground resolution of 30 cm (11.8 in) / pixel, no wind, moderate weather temp. (18 °C/64.4 °F), new fully charged battery, flight altitude of 1,000 m (3,280 ft) above ground level, take off at approx. sea level, take-off point in centre of desired coverage area.

\*\*\* Depends upon environmental conditions (light, wind, surface type).

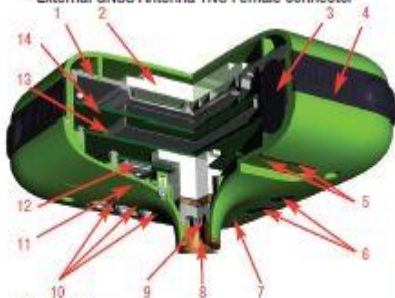


### Package contents:

- eBee body (inc. all electronics & built-in autopilot)
- Pair of detachable wings
- WX still camera (inc. SD card, battery, USB cable & charger)
- 2.4 GHz USB radio modem for data link (inc. USB cable)
- Two lithium-polymer battery packs & charger
- Spare propeller
- Carry case with foam protection
- Remote control & accessories (for safety pilots)
- User manual
- eMotion software download key (accessible via my.senseFly at no extra cost)

## Appendix 5 – Technical Specifications of JAVAD Triumph-1 GNSS

Standard Configuration	Description
<ul style="list-style-type: none"> <li>• GPS L1/L2/L2C/L5</li> <li>• GLONASS L1/L2</li> <li>• Update Rate 5Hz</li> <li>• RTK Rate 5Hz</li> <li>• Memory 256 MB</li> <li>• RAM</li> <li>• Code Differential Base/Rover</li> <li>• Advanced Multipath Reduction</li> <li>• MinPad Interface</li> <li>• Two RS232 Serial Ports (460.8 kbps)</li> <li>• USB port</li> <li>• Internal GNSS antenna</li> <li>• Bluetooth® Interface</li> <li>• Wi-Fi (IEEE 802.11b/g)</li> <li>• KFK WAAS/EGNOS (SBAS)</li> <li>• Rechargeable Li-Ion Battery</li> </ul>	<p>Total 216 channels: all-in-view (GPS L1/L2/L5, Galileo E1/E5A/E5B, GLONASS L1/L2/L5, QZSS L1/L2/L5, Beidou B1/B2, SBAS L1/L5) integrated receiver, rugged plastic and magnesium housing complete with MinPad interface</p>
Optional Feature	Tracking Specification
<ul style="list-style-type: none"> <li>• Galileo E1/E5A</li> <li>• Galileo E5B*</li> <li>• GLONASS L3*</li> <li>• QZSS</li> <li>• Beidou B1</li> <li>• Beidou B2*</li> <li>• Update Rate 10Hz, 20Hz, 50Hz &amp; 100Hz</li> <li>• RTK Rate 10Hz, 20Hz, 50Hz &amp; 100Hz</li> <li>• Data Recording up to 2048 MB</li> <li>• Heading Determination</li> <li>• GLONASS 2mm Dynamic Calibration</li> <li>• In-Band Interference Rejection</li> <li>• JAVAD ArcPad Extension</li> <li>• 1 PPS timing strobe</li> <li>• Event Marker</li> <li>• Internal 3.5G UMTS/HSPA Module</li> <li>• Internal GSM/GPRS/EDGE Module</li> <li>• Internal CDMA2000 Module</li> <li>• Internal UHF Modem</li> <li>• Ethernet</li> <li>• External GNSS Antenna TNC Female connector</li> </ul>	<p>Signals Tracked GPS C/A, P1, P2, L2C (L+M), L5 (I+Q), Galileo E1 (B+C), E5A (I+Q), E5B (I+Q), AltBoc GLONASS C/A, L2C, P1, P2, L3 (I+Q) QZSS C/A, L1C(I+Q), L2C (L+M), L5 (I+Q), SAIF Beidou B1, B2 SBAS L1, L5</p>
	Performance Specifications
	<p>Autonomous &lt;2 m Static, Fast Static Accuracy Horizontal: 0.3 cm + 0.1 ppm + base_line_length** Vertical: 0.35 cm + 0.4 ppm + base_line_length Kinematic Accuracy Horizontal: 1 cm + 1 ppm + base_line_length Vertical: 1.5 cm + 1 ppm + base_line_length RTK (OTF) Accuracy Horizontal: 1 cm + 1 ppm + base_line_length Vertical: 1.5 cm + 1 ppm + base_line_length DGPS Accuracy &lt; 0.25 m Post Processing &lt; 0.5 m Real Time Cold Start &lt;35 seconds Warm Start &lt;5 seconds Reacquisition &lt;1 second</p>
	Power Specification
	<p>Battery Two internal Li-Ion batteries (7.4 V, 5.8 Ah each) with internal charger Operation Time Up to 18 hours External Power Input +10 to +30 volts</p>
	GNSS Antenna Specifications
	<p>GNSS Antenna Integratpd Antenna Type Microstrip (Zero Centered) Ground Plane Antenna on a flat ground plane</p>
	Radio Specifications
	<p>3.5G UMTS/HSPA Module Global (850/1900/2100) /North America (850/1900/1700-2100AWS) / Europe (900/2100) GSM/GPRS/EDGE Module Internal GSM/GPRS/EDGE quad-band module, GPRS/EDGE Class 10 CDMA 2000 Module Internal CDMA2000 dual band module 800/1900MHz UHF Radio Modem Internal 360-470MHz radio transceiver, up to 38.4kbps Base Power Output 1 Watt</p>
	I/O
	<p>Communication Ports 2x serial (RS232) up to 460.8 kbps High speed USB 2.0 device port (480 Mbps) Full-duplex 10BASE-T/100BASE-TX Ethernet port Wi-Fi (IEEE 802.11b/g) Bluetooth V2.0+EDR Class 2 supporting SPP Slave and Master Profiles Other I/O Signals 1 PPS synchronized Event Marker Status Indicator Six LEDs, two function keys (MinPad)</p>
	Memory & Recording
	<p>Internal Memory Up to 2048MB of onboard non-removable memory for data storage Raw Data Recording Up to 100 times per second (100Hz) Data Type Code and Carrier from GPS L1/L2, Galileo E1/E5A, GLONASS L1/L2</p>
	Real Time Data
	<p>Input/Output JPS, RTCM SC104 v. 2.x and 3.x, CMR Output NMEA 0183 v. 2.x and 3.0, BINEX</p>
	Environmental Specifications
	<p>Enclosure Molded magnesium alloy and plastic, waterproof IP67 Operating Temperature -40° C to +60° C*** Storage Temperature -45° C to +95° C*** Humidity 100% condensing Shock Survives a 2 m drop onto hard surface Dimensions W:178 mm x H:96 mm x D:178 mm Weight 1700 g</p>



1. Ground Plane
2. Internal GNSS Antenna
3. Rechargeable Li-Ion Battery Pack
4. Guard Bumper
5. 1PPS and Event Marker Connectors (optional)
6. On/Off and Control Buttons and LEDs
7. Bluetooth / WiFi Antenna
8. 5/8-11" Mounting Thread
9. UHF / GSM / CDMA2000 Antenna Connector
10. Communication and Power Ports
11. SIM/UM Card Door
12. User Accessible SIM/UM Card
13. GNSS Receiver and Power Board with on-board Memory
14. GNSS RF and Communication Board with on-board SIM/UM Card

Specifications are subject to change without notice



**JAVAD GNSS**

\*Based on ISO 9001  
\*\*For good observation conditions and proper length of observation session  
\*\*\*The operating temperature range of Li-Ion batteries is -20°C to +40°C  
\*\*\*\*Storage temperature of Li-Ion batteries is -20°C to +40°C

**Appendix 6 – Details of the Two Data Set (B) and T-Test (A)**

**A) T-Test**

**Paired Samples Statistics**

	Mean	N	Std. Deviation	Std. Error Mean
Pair 1 VAR0000 1	4,8847	53	1,23278	,16933
VAR0000 2	4,8394	53	1,25215	,17200

**Paired Samples Correlations**

	N	Correlation	Sig.
Pair 1 VAR00001 & VAR00002	53	,934	,000

**Paired Samples Test**

	Paired Differences			
	Mean	Std. Deviation	Std. Error Mean	95% Confidence Interval of the Difference
				Lower
Pair 1 VAR00001 - VAR00002	,04528	,28262	,03882	-,03262

### Paired Samples Test

	Paired Differences	t	df	Sig. (2-tailed)
	95% Confidence Interval of the Difference			
	Upper			
Pair 1 VAR00001 - VAR00002	,12318	1,166	52	,249

### B) Two Data Sets

Ground Measurement Based		Algorithm Based	
ID	Height(m)	ID	Height(m)
c1	3,86	c1	4,28
c2	5,23	c2	5,37
c3	5,67	c3	5,69
c4	4,16	c4	3,86
c5	4,65	c5	4,35
d1	4,99	d1	4,79
d2	3,59	d2	3,53
d4	5,54	d4	5,21
g1	1,74	g1	1,27
g11	5,83	g11	5,25
g2	6,05	g2	5,75
g3	4,87	g3	5,28
g4	5,69	g4	5,87
g5	2,49	g5	2,62
g6	2,23	g6	2,34
g7	4,37	g7	4,09
g8	5,35	g8	5,06
g9	5,79	g9	5,67
h1	4,76	h1	5,03
h3	3,59	h3	3,55
h4	3,71	h4	3,53

h5	2,86	h5	2,90
h6	3,72	h6	4,05
h7	2,74	h7	3,21
h8	3,91	h8	3,82
i1	2,58	i1	2,00
i10	7,08	i10	6,79
i11	6,62	i11	6,47
i12	5,70	i12	5,95
i13	5,55	i13	5,26
i2	5,91	i2	6,07
i3	6,11	i3	6,11
i4	5,72	i4	5,79
i5	5,70	i5	5,11
i6	5,53	i6	5,73
i7	6,30	i7	5,84
i8	4,71	i8	4,35
i9	4,87	i9	4,72
j1	5,95	j1	6,25
j2	3,81	j2	3,61
j3	5,46	j3	5,73
j4	6,21	j4	5,93
j5	4,56	j5	4,75
j6	5,62	j6	5,78
j7	6,12	j7	6,22
j8	6,03	j8	5,81
k1	3,26	k1	2,94
k2	5,14	k2	5,32
k3	4,82	k3	5,09
k4	5,41	k4	5,79
k5	4,99	k5	5,23
k6	5,57	k6	5,35
k7	6,17	k7	6,13



## RESUME (in Turkish)

### ANIL CAN BİRDAL ARAŞTIRMA GÖREVLİSİ



<b>E-Posta Adresi</b>	:	anilcanbirdal@hotmail.com
<b>Telefon (İş)</b>	:	3462191010-2467
<b>Telefon (Cep)</b>	:	5075565897
<b>Faks</b>	:	
<b>Adres</b>	:	Cumhuriyet Üniversitesi Mühendislik Fakültesi A Binası Geomatik Mühendisliği Bölümü

### Öğrenim Durumu

Yüksek Lisans 2013	ANADOLU ÜNİVERSİTESİ FEN BİLİMLERİ ENSTİTUSU/UZAKTAN ALGILAMA VE COĞRAFI BİLGİ SİSTEMLERİ ANABİLİM DALI/UZAKTAN ALGILAMA VE COĞRAFI BİLGİ SİSTEMLERİ BİLİM DALI Tez adı: Ağaç Yüksekliklerinin Belirlenmesinde İnsansız Hava Araçlarının Kullanımı (Eskişehir Kent Ormanı Örneği) Tez Danışmanı:(UGUR AVDAN,TARİK TURK)
Lisans 2008-2013	BÜLENT ECEVİT ÜNİVERSİTESİ MUHENDİSLİK FAKÜLTESİ/GEOMATİK MUHENDİSLİĞİ BÖLÜMÜ

### Görevler

ARAŞTIRMA GÖREVLİSİ 2013	CUMHURİYET ÜNİVERSİTESİ/MÜHENDİSLİK FAKÜLTESİ/GEOMATİK MÜHENDİSLİĞİ BÖLÜMÜ/FOTOGRAMETRİ ANABİLİM DALI (27 Eylül 2013 Başlangıç)
-----------------------------	---

### Projelerde Yaptığı Görevler:

- Optik Uydu Görüntüleri Yardımıyla Heyelan Alanlarında Meydana Gelen Yatay Yer Değişikliklerinin Belirlenmesi: Kuzey Anadolu Fay Zonu (Kafz) (Sivas İli Koyulhisar İlçesi ve Çevresi) Örneği. TÜBİTAK Projesi. TÜBİTAK PROJESİ. Bursiver. 2013-2015 (ULUSAL)

### İdari Görevler

Farabi Koordinatörü 2014	CUMHURİYET ÜNİVERSİTESİ/MÜHENDİSLİK FAKÜLTESİ/GEOMATİK MÜHENDİSLİĞİ BÖLÜMÜ/FOTOGRAMETRİ ANABİLİM DALI
Mevlana Değişim Programı Kurum Koordinatörü 2014	CUMHURİYET ÜNİVERSİTESİ/MÜHENDİSLİK FAKÜLTESİ/GEOMATİK MÜHENDİSLİĞİ BÖLÜMÜ/FOTOGRAMETRİ ANABİLİM DALI
Erasmus Koordinatörü 2014	CUMHURİYET ÜNİVERSİTESİ/MÜHENDİSLİK FAKÜLTESİ/GEOMATİK MÜHENDİSLİĞİ BÖLÜMÜ/FOTOGRAMETRİ ANABİLİM DALI

### B. Uluslararası bilimsel toplantılarda sunulan ve bildiri kitaplarında (proceedings) basılan bildiriler :

1. GURSOY ONDER, BİRDAL ANIL CAN, OZYONAR FUAT, KASAKA ERGUN (2015). Determining and Monitoring the Water Quality of Kizilirmak River of Turkey, First Results. 36th International

Symposium on Remote Sensing of Environment (ISRSE) (Berlin/Germany) (Tam metin bildiri)(Yayın No:1706442)

2. POYRAZ FATİH,HASTAOĞLU KEMAL OZGUR,TIRYAKIOĞLU İBRAHİM,TATAR ORHAN,GURSOY ÖNDER,KOÇBULUT FİKRET,TÜRK TARIK,DEMİREL Mehmet,DUMAN HÜSEYİN,AHMET Faruk ÇİĞER,BİRDAL ANIL CAN (2015). The Eastern Part Of Gediz Graben Determination Methods of Tectonic Movements GPS And Ps-InSAR: The First Results. European Geosciences Union General Assembly 2015 (Austria/Vienna) (Poster)(Yayın No:1706009)
3. Demirel Mehmet,POYRAZ FATİH,HASTAOĞLU KEMAL OZGUR,TURK TARIK,TATAR ORHAN,BİRDAL ANIL CAN (2015). Comparing the Results of Terrasar-X And Envisat Sar Images With Ps-InSAR Methods On Slow Motion Landslides: Koyulhisar, Turkey. European Geosciences Union General Assembly 2015 (Austria/Vienna) (Poster)(Yayın No:1706048)
4. TURK TARIK,GORUM TOLGA,BİRDAL ANIL CAN,TATAR ORHAN (2015). Landslide displacement measurements from Optical Satellite Images: A Case Study on the North Anatolian Fault Zone. European Geosciences Union General Assembly 2015 (Austria/Vienna) (Poster)(Yayın No:1706145)
5. GURSOY ÖNDER,BİRDAL ANIL CAN,OZYONAR FUAT,KASAKA ERGUN (2015). The Water Quality Assessment of Kizilirmak River of Turkey: First Results. Mapping Water Bodies from Space - MWBS 2015 (Frascati/Rome/Italy) (Poster)(Yayın No:1706337)

#### E. Ulusal bilimsel toplantılarda sunulan ve bildiri kitaplarında basılan bildiriler:

1. TURK TARIK,GORUM TOLGA,BİRDAL ANIL CAN (2015). Optik Uydu Görüntüleriyle Heyelan Alanlarında Ki Kütle Hareketlerinin İncelenmesi: Kuzey Anadolu Fay Zonu Örneği. Türkiye Ulusal Fotogrametri ve Uzaktan Algılama Birliği (TUFUAB) VIII. Sempozyumu (Konya), (Yayın No:1705745)
2. GURSOY ÖNDER,BİRDAL ANIL CAN (2014). Farklı Uydu Verilerinin Bant Birleştirilmesinden Sonra Spektral Sınıflandırmalarda Kullanılması. 5. Uzaktan Algılama-Coğrafi Bilgi Sistemleri Sempozyumu (İstanbul), (Yayın No:1705530)
3. Y. YAZAR, U. AVDAN, A. BİRDAL, M, TUN (2010). Mimari Belgelemede Lazer Tarama Uygulamaları (Kurşunlu Külliyesi Okuma Salonu Örneği). Harita ve Kadastro Mühendisleri Odası, Mühendislik Ölçmeleri STB Komisyonu 5. Ulusal Mühendislik Ölçmeleri Sempozyumu (Zonguldak), 263-264, (Yayın No:891165)

#### Üniversite Dışı Deneyim

2012-2012	<b>Harita Mühendisi</b>	İnan Harita, Hali Hazır Harita, (Ticari (Özel))
2011-2011	<b>Stajer</b>	Laser Scanning Europe Şirketi (Magdeburg/Almanya), Stajer, (Diğer)
2010-2010	<b>Stajer</b>	Anadolu Üniversitesi Yer ve Uzay Bilimleri Enstitüsü, Stajer, (Diğer)